BOREAS An international journal of Quaternary research

Drivers of glacially induced fault reactivation in the Baltic Sea sector of the Tornquist Fan

ELISABETH SEIDEL, HOLGER STEFFEN, REBEKKA STEFFEN, NIKLAS AHLRICHS AND CHRISTIAN HÜBSCHER

BOREAS

Seidel, E., Steffen, H., Steffen, R., Ahlrichs, N. & Hübscher, C. 2025 (April): Drivers of glacially induced fault reactivation in the Baltic Sea sector of the Tornquist Fan. *Boreas*, Vol. 54, pp. 220–245. https://doi.org/10.1111/bor.12689. ISSN 0300-9483.

We analyse the effect of Quaternary glaciations on the complex tectonic pattern within the southwestern Baltic Sea, a sector of the transition zone from the East European Craton to the West European Platform. This area comprises the Caledonian Trans–European Suture Zone in the south and the Tornquist Zone in the north. Multiple fault zones in between, with different strike and dip angles, and characters (normal, thrust/reverse, strike-slip), document like scars the alternately transpressional and transtensional stress activities since the Palaeozoic. We determine the strike directions and dip angles of more than 40 potential glacially reactivated faults identified in 2D marine reflection seismic data. Finite element simulations of different glacial isostatic adjustment models provide glacially induced Coulomb failure stress changes (ΔCFS) at the faults over time, starting 200 000 years ago (200 ka, Saalian phase) up to 1000 years into the future. Assuming strike-slip or thrust/reverse background stresses, a potential reactivation of each fault is analysed. The detected reactivation phases are related to the waxing and waning ice masses (Late Saalian ice advances: *c.* 170–135 ka ago; Weichselian ice advances: 70–60, 45–38, 26–14 ka ago) and point to an activation in front of the ice margin. Comparing the ΔCFS results of the individual faults laterally and over time, we found that the location of the fault, depending on its position during a glacial maximum, has an important effect on its reactivation potential. The closer a fault was located to the former ice margin, the higher was the glacially induced stress during the ice retreat. Based on earlier findings in Germany and Denmark, glacially triggered faults are a typical consequence of the Fennoscandian glaciation throughout northern central Europe, and this also applies to future glaciation phases.

Elisabeth Seidel (elisabeth.seidel@uni-hamburg.de), Niklas Ahlrichs and Christian Hübscher, Institute of Geophysics, Center for Earth System Research and Sustainability, University of Hamburg, Bundesstrasse 55, 20146 Hamburg, Germany; Holger Steffen, Lantmäteriet, Lantmäterigatan 2C, 801 82 Gävle, Sweden; Rebekka Steffen, Lantmäteriet, Lantmäterigatan 2C, 801 82 Gävle, Sweden and Department of Earth and Environmental Sciences, Dalhousie University, 6287 Alumni Cres, PO BOX 15000, Halifax, Nova Scotia B3H 4R2, Canada; *present address: Ramboll Denmark A/S, Hannemanns Allé 53, 2300 Copenhagen, Denmark;* *received 17th June 2024, accepted 14th November 2024.*

Faulting can be induced by both endogenetic forces, such as tectonic stress within the lithosphere from plate motion, and exogenetic forces, including glacial movements, landslides, and human activities. In northern Europe, the stress field is dominated by a combination of exogenetic glacial isostatic adjustment (GIA) and endogenetic lithostatic and tectonic stress regimes. GIA is a process where the Earth adjusts its shape in response to the waxing and waning of ice sheets. The large (some 10 MPa) glacially induced stress changes within the Earth's crust can potentially trigger the reactivation of faults, leading to enhanced seismic activity and thus an earthquake hazard. Moreover, due to the propensity for fault reactivation over new fault generation, even minor stress changes, in the order of a few kPa, can lead to the reactivation of faults, whether optimally or non-optimally orientated within a stress field (King *et al.* 1994; Steffen *et al.* 2021a, b).

Glacially induced faults (GIF) have been studied in northern and northern central Europe (e.g. Müller *et al.* 2020, 2021; Olesen *et al.* 2021; Pisarska-Jamroży *et al.* 2021; Sandersen *et al.* 2021; Smith *et al.* 2021; Sutinen *et al.* 2021), Canada (e.g. Adams 1989; Brooks & Adams 2020), Alaska (Sauber *et al.* 2021) and the polar region (Steffen *et al.* 2020; Steffen & Steffen 2021a). These studies focused dominantly on the mainland (onshore) and used several approaches to date fault reactivation. In addition to the standard stratigraphical approach (a fault has the same age or younger as the youngest succession that it is displacing and wherein it terminates), optically stimulated luminescence (OSL) dating and model simulations of the Coulomb failure stress change (ΔCFS) were used to estimate the effect of glacially induced stress on the reactivation potential of individual faults and the time when reactivation was possible or not (Brandes *et al.* 2012, 2018; Steffen *et al.* 2014, 2019; Pisarska-Jamroży *et al.* 2019, 2022; Štěpančíková *et al.* 2022).

In northern Germany, which is also affected by GIA, Quaternary fault activation and reactivation have been studied since the early 20th century (e.g. Philippi 1906; Keilhack 1912; Steinich 1972). During recent years, there has been a resurgence of interest in this topic, driven by the search for tectonically quiet sites for underground storage or offshore wind farm constructions. The investigation of GIF or soft-sediment deformation structures focused mainly on an area between the northern border of the Tornquist Zone to the Low Mountain range in central Germany (Harz Mountains; e.g. Brandes *et al.* 2012, 2018, 2022; Pisarska-Jamroży *et al.* 2019, 2022; Grube 2019a, b; Müller *et al.* 2020).

DOI 10.1111/bor.12689

In this study, we focus on the southwestern Baltic Sea, which can be seen as the marine gap area between the Tornquist Zone and the onshore Danish and German GIF studies. The southwestern Baltic Sea comprises geographically the area between the Bay of Kiel in the west and the Pomeranian Bay in the east. Our understanding of its regional tectonics is well established: the continental crust comprises a multitude of faults that were mapped in detail by numerous offshore seismic campaigns (e.g. Krzywiec *et al.* 2003; Hübscher *et al.* 2004, 2010; Hansen *et al.* 2005, 2007; Zöllner *et al.* 2008; Al Hseinat *et al.* 2016; Kammann *et al.* 2016; Al Hseinat & Hübscher 2017; Seidel *et al.* 2018; Ahlrichs *et al.* 2020, 2021, 2023a, b; Huster *et al.* 2020; Pan *et al.* 2022). The big advantage of these non-invasive offshore seismic measurements is the free profile orientation, so that e.g. faults can be crossed perpendicularly, without having to consider infrastructure or morphology.

The complex fault pattern within the southwestern Baltic Sea includes a variety of tectonic features differing in age, strike direction, and vertical or lateral extension. In a regional tectonic sense, the area is located above the northern marginal part of the Trans–European Suture Zone (e.g. Guterch et al. 2010). This area acted like a hinge between the stable part of Baltica (East European Craton) and the West European Platform, and compensated the alternating tectonic stresses. The Baltic Sea region is also located at the northern border of the intracontinental North German Basin (NGB) that formed during the Palaeozoic to Mesozoic (e.g. Guterch *et al.* 2010). Intense salt tectonics and Cretaceous to Palaeogene inversion processes complete the complex structural-geological situation (e.g. Warsitzka et al. 2019; Pan et al. 2022).

During the Quaternary, at least three major glaciations modified the relief of the later Baltic Sea: the Elsterian, the Saalian and predominately the Weichselian glaciations. The phases of ice advance and retreat are known for fault reactivation, which lasts until today due to ongoing isostatic adjustments (e.g. Brandes *et al.* 2012, 2018; Pisarska-Jamroży *et al.* 2019, 2022; Steffen *et al.* 2019, 2021a). An effect of ice loading on the reactivation of supra-salt has been conceptually described by Sirocko *et al.* (2008) and further analysed by Lang *et al.* (2014) and Lang & Hampel (2023).

In this study, we use known faults from previous seismic studies in the Baltic Sea, identify which of these faults dissect the base of the Quaternary or the sea floor, and thus have been potentially reactivated in glacial times (focusing on the last 200 000 years (200 ka)). Using the seismic data, we estimate fault properties and analyse them regarding their potential glacial reactivation by combining them with glacially induced Coulomb failure stress changes (ΔCFS) calculated with a set of GIA models. This method, providing stress changes at the faults over time, has previously mostly been used for onshore data and single faults mapped at outcrops. We adapt this method for our offshore data set with multiple optimally and non-optimally orientated faults, addressing the following questions: (i) Did the Saalian and Weichselian glaciation lead to fault reactivation in the southwestern Baltic Sea? (ii) Why are some faults in the southwestern Baltic Sea prone to potential glacially induced reactivation and some not? (iii) How do the dimension and shape of the ice sheet affect glacially reactivated faulting? (iv) Is there a certain stress and GIA model combination for which many faults indicate potential glacially induced fault reactivation in the southwestern Baltic Sea? (v) Do the results correlate with other glacially induced fault reactivations discussed in Germany and Denmark? (vi) How does a possible reactivation of this multitude of faults fit into the picture of the palaeoseismicity and the present seismicity of the area?

Answering these questions is not only important from a scientific point of view but also from a societal one since Denmark and Germany are in the search process for potential areas for long-term disposal of radioactive waste, for which the integrity of the host rock must be guaranteed for a period of up to 1 million years (a period that will probably include future ice ages; BGE 2024). Moreover, the results can be used for risk assessment for CO_2 storage, geothermal energy, and windfarm construction sites. Ultimately, the results can be applied to regions that are currently covered by ice sheets but experiencing rapid climatic change, such as the polar regions (Steffen & Steffen 2021a and references therein).

Geological overview

Ordovician to Tertiary evolution and structural features

The Caledonian Trans–European Suture Zone (TESZ) represents the transition from the Precambrian East European Craton (EEC) in the northeast to the West European Platform (WEP, with Palaeozoic lithosphere) in the southwest (Guterch *et al.* 2010). The suture strikes northwest–southeast and contains the area between the Caledonian Deformation Front (CDF, northernmost front of the Caledonian accretionary wedge) in the north and the Elbe Line in the south (summarized e.g. by Guterch *et al.* 2010). The Tornquist Zone (Fig. 1) comprises the Sorgenfrei–Tornquist Zone (STZ), trending from the North Sea southeastward until Bornholm Island, and the Teisseyre–Tornquist Zone (TTZ), trending from Bornholm Island until the Black Sea (e.g. Erlström *et al.* 1997; Ponikowska *et al.* 2024). Both branches are horizontally displaced at the Rønne Graben (Fig. 1). The TESZ and the Tornquist Zone approach each other in Poland and continue their strike towards the southeast almost parallel to each other (Fig. 1). Therefore, the general nature of the Tornquist Zone and of the TTZ in particular has been widely discussed in recent years (e.g. Znosko 1979; Erlström *et al.* 1997;

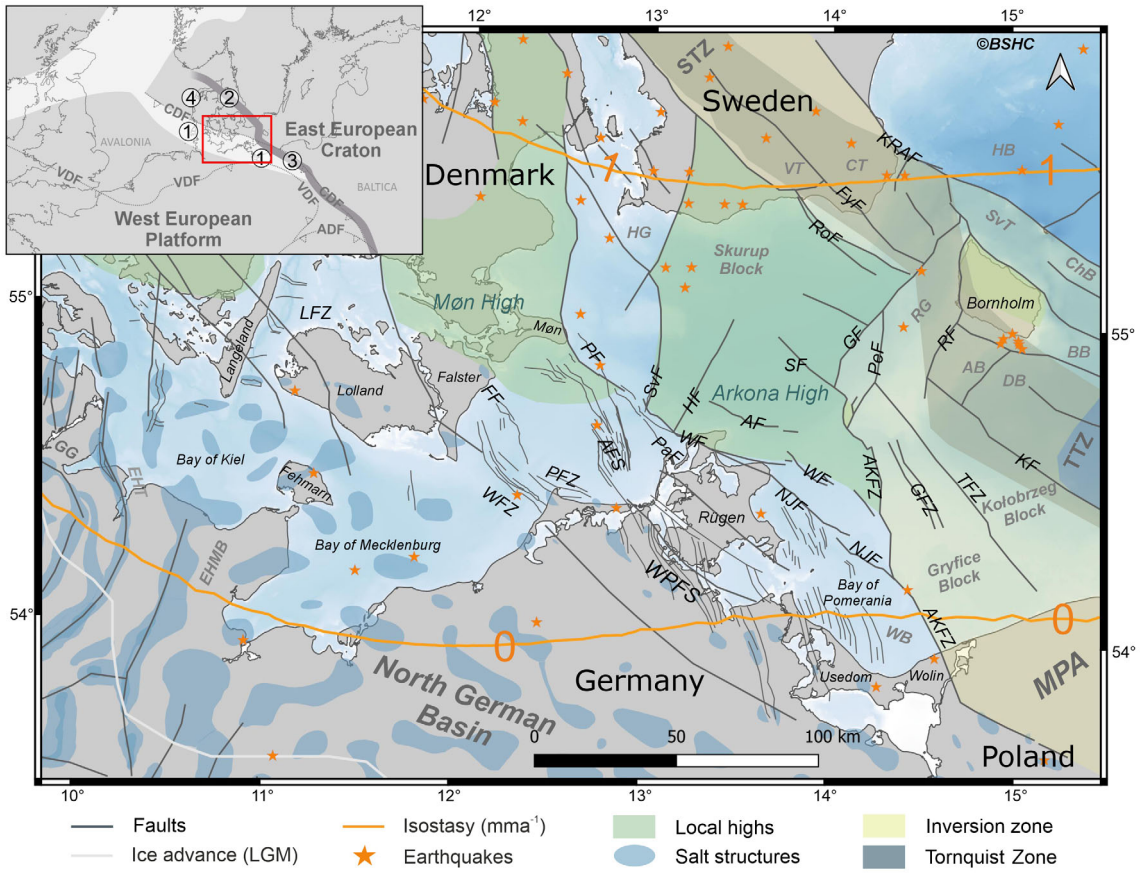

Fig. 1. Structural overview of our study area with the Weichselian ice margin 23 000–21 000 years BP (Houmark-Nielsen *et al.* 2005), isobases of land uplift (0 and 1 mm a^{-1}, model NKG2016LU_abs; Vestøl *et al.* 2019), the location of recent earthquakes (Deutscher Erdbebenkatalog,©BGR, Hannover 2012), and structural units are redrawn and modified according to Vejbæk & Britze (1994), Schlüter *et al.* (1997), Krzywiec *et al.* (2003), Nielsen (2003), Krauss and Mayer (2004), Seidel *et al.* (2018), Warsitzka *et al.* (2019), and Ahlrichs *et al.* (2021, 2023b and citations therein). The Tornquist Zone (grey polygon) and the horst-and-graben zone of Cretaceous to Palaeogene inversion (yellow) are differentiated and slightly modified according to Ponikowska *et al.* (2024). The bathymetry is based on the Baltic Sea Hydrographic Commission (2013). The overview map in the upper left is based on Thybo (2000), Meschede and Warr (2019) and Ponikowska *et al.* (2024), visualizing the location of: 1 – Trans–European Suture Zone, 2 – Sorgenfrei–Tornquist Zone, 3 – Teisseyre–Tornquist Zone, 4 – Tornquist Fan. Red rectangle shows the location of the study area (ADF = Alpine Deformation Front; CDF = Caledonian Deformation Front; VDF = Variscan Deformation Front). Abbreviations in main map: AB = Arnager Block; AF = Arkona Fault; AFS = Agricola Fault System; AKFZ = Adler-Kamień Fault Zone; BB = Bornholm Block; ChB = Christiansø Block; CT = Colonus Shale Trough; DB = Darłowo Block; EHMB = Eastholstein–Mecklenburg; EHT = Eastholstein Trough; FF = Falster Fault; FyF = Fyledalen Fault; GF = Gat Fault; GFZ = Gryfice Fault Zone; GG = Glückstadt Graben; HB = Hanö Block; HF = Hiddensee Fault; HG = Höllviken Graben; KF = Koszalin Fault; KRAF = Kullen-Ringsjön-Andrarum Fault; LFZ = Langeland Fault Zone; MPA = Mid-Polish Anticlinorium; NJF = Nord Jasmund Fault; PaF = Parchim Fault; PeF = Pernille Fault; PF = Plantagenet Fault; PFZ = Prerow Fault Zone; RF = Rønne Fault; RG = Rønne Graben; RoF = Romeleåsen Fault; SF = Skurup Fault; SvF = Svedala Fault; STZ = Sorgenfrei–Tornquist Zone; SvT = Svaneke Trough; TFZ = Trzebiatów Fault Zone; TTZ = Teisseyre–Tornquist Zone; WB = Wolin Block; WF = Wiek Fault; WFZ = Werre Fault Zone; WPFS = Western Pomeranian Fault System; VT = Vomb Trough.

Thybo 2000; Krzywiec 2009; Mazur *et al.* 2015, 2018; Narkiewicz *et al.* 2015; Ponikowska *et al.* 2024). Especially the STZ but also the TTZ were attributed to the deep fracture zone (e.g. Erlström *et al.* 1997). However, other publications discussed the TTZ as the southeastern border of the EEC (e.g. Narkiewicz *et al.* 2015). Most recently Ponikowska *et al.* (2024) defined the Tornquist Zone as an intra-cratonic feature of crustal thickening. The northwestward widening area comprising the Tornquist Zone in the north and the northwestern part of the TESZ in the south is known as the Tornquist Fan (Thybo 1997, 2000, 2001; cf. Fig. 1).

The collapse of the German-Polish Caledonides was followed by post-Caledonian extension, Variscan compression, Permian volcanism and thermal subsidence, break-up of Pangaea and transtension from Permian to Early Cretaceous times (e.g. Pharaoh *et al.* 2010). Some faults of the northwest-trending fracture zone (e.g. Gryfice Graben, Rønne Graben, Colonus Shale Trough) formed during the Permo-Carboniferous (Erlström *et al.* 1997; Thybo 2000, 2001). Especially the Late Palaeozoic and Mesozoic were characterized by the formation and differentiation of the intracontinental Central European Basin System and in particular of the

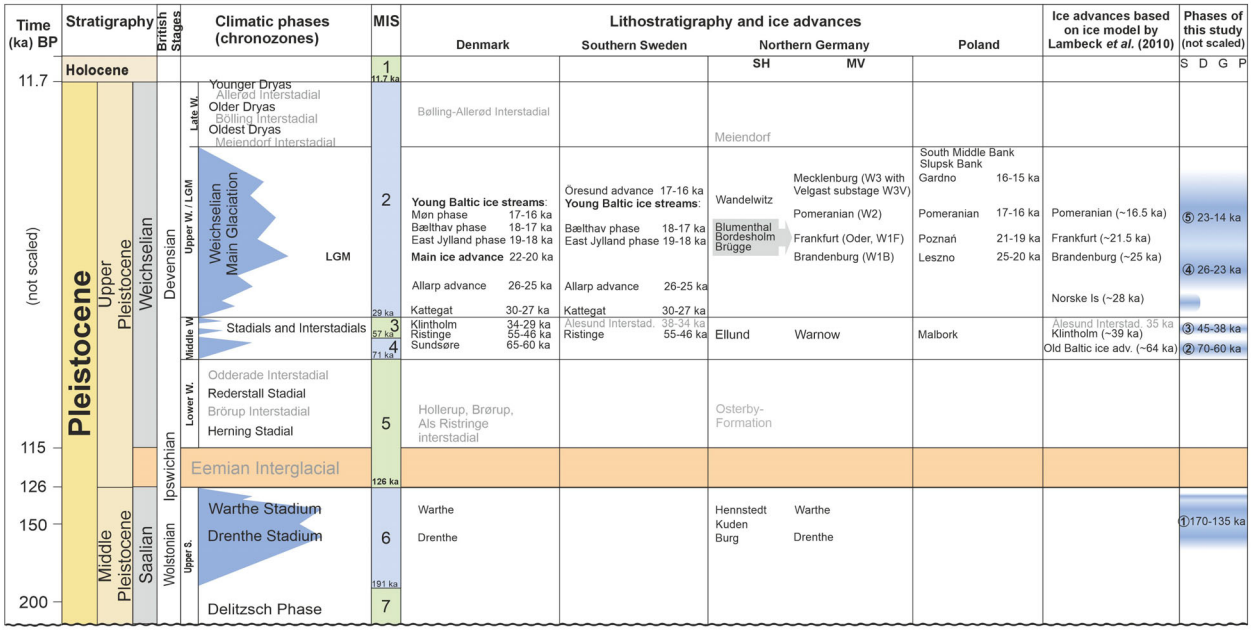

Fig. 2. Stratigraphical table of the past 200 000 years. The stratigraphy and climatic phases are based on the German Stratigraphic Commission (2016), the marine isotope stages (MIS) on Cohen & Gibbard (2012 and references therein), and bold times on the German Stratigraphic Commission (2016). Warm stages are green, cold ones are blue. The informations on 'Lithostratigraphy and ice advances' are summarized according to Müller (2007), Anjar *et al.* (2010, 2014), Houmark-Nielsen (2010, 2011), Böse *et al.* (2012), Stephan (2014), Börner *et al.* (2019). The ages given are mostly approximate values. D = Denmark; G = Germany; ka = 1000 years; LGM = Last Glacial Maximum; MV = Mecklenburg Vorpommern/engl. Mecklenburg Western Pomerania; P = Poland; S = Sweden; SH = Schleswig-Holstein; Upper S. = Upper Saalian; W. = Weichselian. Phases of this study: 1 = Late Saalian; 2 = MIS 4; 3 = MIS 3; 4 = Main Weichselian glaciation 1 (MWG 1); 5 = Main Weichselian glaciation 2 (MWG 2).

deepening North German Basin (NGB), Mid-Polish Trough and Rønne Graben (Scheck-Wenderoth *et al.* 2008; Pharaoh *et al.* 2010). East–west extension forced the formation of the Glückstadt Graben (west of the study area; Warsitzka *et al.* 2019). Contemporaneously, the crustal scale inherited fault and graben zone in the northern extension of the Polish Trough formed in the eastern study area (we will focus on the Vomb Trough, the Colonus Shale Trough, the Christiansø Block, the Rønne Graben, the Gryfice Graben and the Kołobrzeg Graben; Pharaoh *et al.* 2010). Due to the remaining stress system in the Mesozoic, transtensional faults formed along the northern NGB margin, such as the northwest–southeast trending Western Pomeranian Fault System (Krauss & Mayer 2004). Salt tectonics of the Zechstein salt successions were triggered by the regional extension within the NGB (Warsitzka *et al.* 2019). Different salt pillows with crestal grabens above are known in the bays of Kiel and Mecklenburg (cf. Fig. 1; for more information see e.g. Warsitzka *et al.* 2019; Huster *et al.* 2020; Ahlrichs *et al.* 2021). Further south and southwest, bigger salt walls strike parallel to faults, such as along the north–south trending faults of the Glückstadt Graben (e.g. Scheck-Wenderoth *et al.* 2008).

During the Late Cretaceous and Palaeogene, northeast–southwest to north–south orientated compression affected northern Europe originating from the Africa-Iberia-Europe Convergence (Kley & Voigt 2008; Kley 2018). According to Ponikowska *et al.* (2024) the Tornquist Zone formed a mechanical buffer and compressional stresses led to inversion of several basin and graben structures in the upper crust. The resulting horst-and-graben structure, close to the strike of the Tornquist Zone, is known as one of the northernmost structures that document reverse fault reactivation, e.g. at the Kullen-Ringsjön-Andrarum Fault (Al Hseinat & Hübscher 2017; Pan *et al.* 2022). Major anticlines formed also due to graben inversions within the Rønne Graben (e.g. Graversen 2004), along the northwest-trending Adler-Kamień Fault Zone, and the Trzebiatów Fault (Ponikowska *et al.* 2024 and citations therein). This Late Cretaceous to Palaeogene inversion zone is highlighted yellow in Fig. 1. The Gryfice and Kołobrzeg anticlines are assigned to the Mid-Polish Anticlinorium (Krzywiec *et al.* 2022; Ponikowska *et al.* 2024).

Quaternary evolution of the southern Baltic Sea

During the Quaternary, at least three major glaciations modified the relief of the later Baltic Sea, namely the Elsterian, the Saalian and the Weichselian glaciations. Thereby at least two ice sheets, which can be separated based on their origin, have to be considered: (i) The

Scandinavian Ice Sheet (SIS) with individual ice streams via the Bothnian/Baltic depression, following the former Eridanos River, which has drained the Baltic depression since the late Cenozoic in a southwest direction (Overeem *et al.* 2001), and via the Skagerrak-Kattegat trough, streaming southward towards Denmark (Houmark-Nielsen 2011). Thus, we differentiate between a southeastward and a southward advancing ice stream. (ii) The British–Irish Ice Sheet (Hughes *et al.* 2016) covered the southwestern part of the North Sea but did not reach the Baltic Sea and is not further considered here.

We limit our study to the glacial history between the late Middle and Late Pleistocene (lasting 200 ka, cf. Fig. 2), thus between the late Marine Isotope Stages (MIS) 6 and 2 (Cohen & Gibbard 2012). This choice is based on the ice model by Lambeck *et al.* (2010) used in our modelling, which covers this time-span. According to Lambeck *et al.* (2010), 'the compilation of the ice margins was completed in 2004'. Of course, the timing and classification of individual ice advances, particularly those predating the Last Glacial Maximum (LGM), have been refined since then, and thus especially regarding interpretation of our results for older glaciation phases we advise caution. We summarize the glacial history in Fig. 2, supplemented by the glacial stages and subunits of more recent publications with the corresponding MIS.

In northern Germany and Denmark, the Late Saalian is subdivided into the Drenthe and Warthe phases (e.g. Houmark-Nielsen 2011). The Drenthe ice advance (*c.* 160 ka ago) was formed by an ice stream that moved through Denmark from the northeast (Houmark-Nielsen 2004, 2011; Houmark-Nielsen *et al.* 2005). During the Warthe Stadium (150–130 ka ago; Litt *et al.* 2007), an ice stream transgressed the southern Baltic Sea area from the east. Later, this ice stream extended across Denmark from the east to east-southeast (Houmark-Nielsen 2004, 2011). Also, the ice model always shows two maxima that might correspond with the so far not precisely dated Drenthe (based on the ice model estimated as 170–150 ka) and the Warthe stadiums (based on the ice model estimated as 150–135 ka). According to the ice model the ice stream advanced from the northeast, through the Baltic channel and retreated in a north-northeast direction (170–135 ka ago; Fig. S1A). A very short third ice advance from the north-northeast might have collapsed north of Rügen Island between 137–135 ka ago.

The Eemian Interglacial and the Early Weichselian occupied the MIS 5, a global warm phase with marine conditions (cf. Fig. 2; Larsen *et al.* 2009; Cohen & Gibbard 2012; German Stratigraphic Commission 2016; Menning 2018). The following Middle Weichselian included the global cold MIS 4 and global warm MIS 3. Lambeck *et al.* (2010 and citations therein) correlated the Old Baltic Ice Advance in Denmark with the MIS 4 (Fig. 2). Moreover, the Danish Ristinge and the Swedish Göteborg I advances appeared contemporaneous, peaking at about 64 ka ago. Later publications (after 2004; e.g. Houmark-Nielsen 2011) referred to the Sundsøre ice advance that extended across northern Denmark from the north between 65–60 ka ago. Thereby the SIS also filled the Norwegian Channel and the Skagerrak-Kattegat depression (Larsen *et al.* 2009; Houmark-Nielsen 2011). The ice model also shows an MIS 4 advance between 70 and 60 ka ago (Fig. S1B) that proceeded from the northeast/east-northeast.

In Germany, the Warnow advance is attributed to the MIS 4 (German Stratigraphic Commission 2016). According to Müller (2007 and citations therein), the Warnow formation could be in genetic correlation with the Ellund advance in Schleswig-Holstein (northwest Germany; Stephan 2014) and the Polish Malbork Phase. In Denmark, however, three Middle Weichselian ice advances are distinguished: Sundsøre (MIS 4), Ristinge and Klintholm (both MIS 3; Houmark-Nielsen 2011). Houmark-Nielsen (2010) summarised a stratigraphical correspondence of the Warnow and Ellund advances with the Baltic Ristinge advance during the MIS 3. However, according to Börner *et al.* (2019) and Kenzler *et al.* (2018), glacial deposits of a Middle Weichselian ice advance are missing in northeast Germany and even absolute ages could not be measured so far. Therefore, the stratigraphical position of the Warnow Phase is still not proven. According to the ice model the MIS 3 ice advance passed through the study area from the northeast to east (45–38 ka; Fig. S1C), reached the Tornquist Zone and proceeded in a westerly direction.

Lambeck *et al.* (2010) differentiated an older MIS 3 interstadial in their ice model, with e.g. the Swedish Tärandö and Danish Glinde phases, peaking around 49 ka ago. This was followed by a MIS 3 stadial (39 ka ago, with the Danish Klintholm and the Swedish Göteborg II), and a younger MIS 3 interstadial known as the Norwegian Ålesund, the Danish Møn or the Swedish Gärdslöv phase, culminating around 35 ka ago (Lambeck *et al.* 2010). However, due to the uncertainties, we will stick to 'MIS 4' and 'MIS 3' advances in the following.

Following the late MIS 3 the Kattegat ice stream prograded from the north across the Kattegat ice lake until central Denmark and further east across southern Sweden (Larsen *et al.* 2009; Houmark-Nielsen 2011), but not in the recent Baltic Sea area. Therefore, it is not considered as a separate phase for GIF reactivation in this study. Lambeck *et al.* (2010) described this first Late Weichselian stadial as the Norske Is or Norwegian phase. The recent area of the southern Baltic Sea region remained ice free. Houmark-Nielsen (2011) categorised the Kattegat advance for the same time period (30–27 ka ago). During the following short interstadial, the ice also retreated from northern Denmark and southern Sweden (Houmark-Nielsen 2011). The main Weichselian (Vistulian) glaciation took place during the global cooling during the MIS 2. It is characterized by an

oscillating ice stream from the northeast, reaching a first maximum extent between 25–20 ka ago that corresponds with the Brandenburg and Frankfurt ice margin in Germany, and the Leszno and Poznań ice margins in Poland (Böse *et al*. 2012; Börner *et al*. 2019 and citations therein). In Denmark, the main ice advance reached its maximum extent 22–20 ka ago (Houmark-Nielsen 2011).

During the following 10 000 years, the extent of the Scandinavian Ice Sheet varied dramatically, and local ice advances differed in time and extent. In southern Sweden and Denmark, the main ice advance was followed by the Young Baltic Ice Stream (Houmark-Nielsen 2011; Anjar *et al*. 2014). The latter is further subdivided into the East Jylland and Bælthav phases. In Denmark, a third phase, known as the Møn phase, is additionally attributed to this phase. Concurrently, the Äresund advance is recognized in the Baltic depression, east of Denmark (Houmark-Nielsen 2011; Anjar *et al*. 2014). Further south in Germany and Poland, the ice sheet extended as well and formed almost at the same time the ice lobes of the Pomeranian phase (17–16 ka ago; Germany and Poland) and the Mecklenburg phase (Germany, known in Poland as Gardno phase; Böse *et al*. 2012 and citations therein).

The ice model by Lambeck *et al*. (2010) represents the LGM slightly different. The Brandenburg/Leszno phase (peaking at 25 ka ago) advanced from the north-northeast to northeast. The alternating ice margin advanced again during the Frankfurt/Poznań (21.5 ka ago) and Pomeranian phases (16.5 ka ago) from the northeast and then turned again to follow a westerly direction (Fig. S1D–F). Due to the ice retreat at *c.* 23 ka ago, we see a clear difference in the ice model between the Brandenburg/Leszno phase (hereafter referred to as Main Weichselian Glaciation – MWG 1), and the Frankfurt, Pomeranian and Mecklenburg phases (hereafter referred to as Main Weichselian Glaciation 2 – MWG 2). According to the ice model, the study area has remained ice free since 14 ka ago.

The present-day stress pattern and recent earthquakes

In northern Europe, major tectonic stresses result from the Alpine-Carpathian Orogeny and the North Atlantic ridge push, which are assumed to be constant over time periods of up to 200 ka (Pharaoh *et al*. 2010 and citations therein). Ahlers *et al*. (2021, 2022) estimated the prevailing stress field in central Europe by fitting results from finite element simulation to data from the World Stress Map project (Heidbach *et al*. 2018). They found a north–south directed maximum stress direction ($S_{H_{max}}$) for northern Germany with a strike-slip faulting stress regime in the upper 1500 m and a normal faulting stress regime below this depth. The stress direction is subject to minor uncertainties for the southern Baltic Sea, but these uncertainties increase towards the north (Kattegat). Fault plane solutions of earthquakes in southern Sweden, which were not included in the model of Ahlers *et al*. (2021), revealed a north-northwest to south-southeast directed compressional stress field (Voss *et al*. 2009).

Northern Germany and the southwestern Baltic Sea region are tectonically and seismically quiet, compared to other regions of the world (Fig. 1). Earthquakes with a maximum magnitude not exceeding 5.5 tend to occur in the Swedish part of the STZ, or further northwest in the Kattegat and the Danish region between the STZ and the Ringkøbing-Fyn High (Voss *et al*. 2009, 2017). The Tornquist Zone is seen as a boundary that separates 'Younger Europe' with earthquakes, from 'Older Europe' with no significant earthquake activity (Gregersen *et al*. 1995).

Material and methods

Seismic data

During the RV 'Maria S. Merian' cruise MSM52 in 2016, the BalTec survey was conducted by the University of Hamburg, in cooperation with the Federal Institute for Geosciences and Natural Resources (BGR), University of Greifswald, Polish Academy of Sciences, Uppsala University and the German Research Centre for Geosciences Potsdam (Hübscher *et al*. 2016; Fig. 3). Due to the special survey setup and the customized processing workflow, the seismic sections have a continuous high resolution from the sea floor until the base of the Zechstein (see Ahlrichs *et al*. 2020, for a detailed description of survey setup and processing flow). Moreover, this data set of 3500 km of high-resolution multichannel seismic data covers the entire southern Baltic Sea, from the western Bay of Kiel until Bornholm and the Polish territorial waters in the east.

These seismic sections link the different pre-existing surveys, all time-migrated 2D reflection seismic profiles and acquired within the last 40 years, horizontally and even vertically (Seidel *et al*. 2018; Ahlrichs *et al*. 2021 and citations therein). The Petrobaltic data set is a reflection seismic survey focussing on the deeper subsurface with a penetration depth in two-way travel time (TWT) of up to 4000 ms (e.g. Rempel 1992). The upper 500 ms (TWT) of these sections are of low resolution. Additional seismic data, focussing on the upper 1500 ms (TWT), were acquired during the BaltSeis and NeoBaltic projects from 1998 to 2004, a collaboration between the Universities of Aarhus and Hamburg (Hübscher *et al*. 2004). Moreover, since 2005 annual student expeditions of the University of Hamburg provided further data sets, which closed data gaps in the southern Baltic Sea systematically (e.g. Hansen *et al*. 2007; Al Hseinat & Hübscher 2014, 2017; Hübscher *et al*. 2019; Ahlrichs *et al*. 2020, 2023a, b).

The stratigraphical and tectonic interpretation in this study follows the previous studies in the southern Baltic

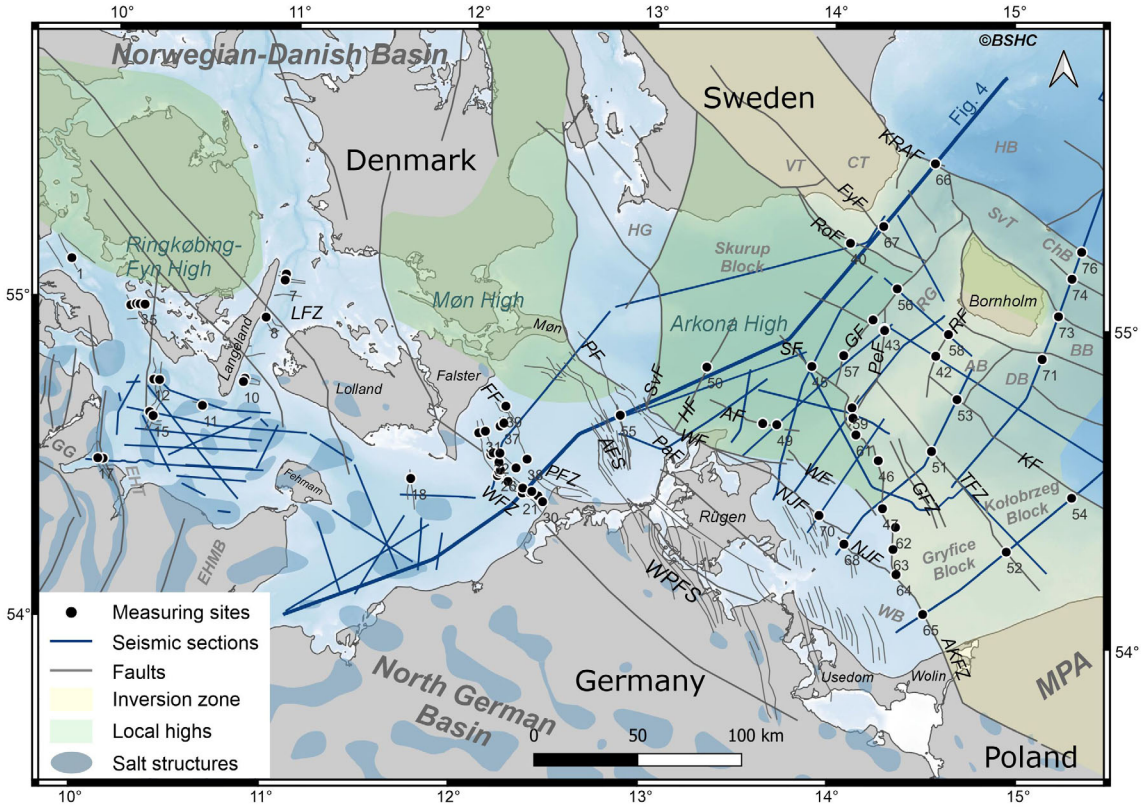

Fig. 3. Location of the MSM52 seismic sections and fault measuring sites 1–76 (black dots). For abbreviations and references see Fig. 1. The thick blue line shows the location of the seismic profile presented in Fig. 4.

Sea (bays of Kiel and Mecklenburg, west of Rügen Island: Al Hseinat and Hübscher 2017; Ahlrichs *et al.* 2020, 2021, 2023a, b; offshore Rügen Island: Seidel *et al.* 2018; Bornholm Gat area: Pan *et al.* 2022).

Preparatory work and structural analysis

We discovered 76 locations of 44 Quaternary reactivated faults, related to different tectonic units, which we used for strike and dip determination (Fig. 3). Indications for Quaternary reactivation were found along Cretaceous inverted anticlines, which are dominantly related to basement block faulting (e.g. at the Mid-Polish Anticlinorium and northern inversion zone; cf. Fig. 1). Furthermore, the Mesozoic transtensional fault zones, like the Western Pomeranian Fault System, or the crestal grabens, relating to salt structures in the NGB, have been reactivated during the Quaternary. In many cases, these faults displace the base of the Quaternary. A few faults also reach very close to the sea floor, some even seem to displace it (Fig. 4D). However, the resolution is not high enough to make reliable statements in these cases. Figure 4 shows a 317-km-long profile, crossing the southern Baltic Sea from southwest to northeast, west of Rügen Island. It crosses all these different tectonic features.

Table 1 summarizes all measured and calculated parameters (fault trend, dip direction, dip angle and dedicated fault zone/system), according to their serial numbers (FIDs). In addition to the FID, each fault has a number and in each case, the fault was measured at several locations (by several profiles, crossing that fault); these locations were labelled by an additional vertex number (cf. Table 1). At each FID we noted the coordinates and the strike and dip directions as well as the dip angles of the faults. The orientation of the faults varies between 0°/360° representing north and measured in a clockwise direction (90° = east, 180° = south, 270° = west). For the ΔCFS analysis, the strike direction was converted to a half-circle domain (0–180°) because the distance between the midpoints of both possible fault surfaces is very small compared to the resolution of the finite element model. Moreover, to ease and speed up the ΔCFS analysis, the strike directions and dip angles were grouped into 15° intervals between 0°–90° for the dip angles and 0°–180° for the strike direction, resulting in a maximum deviation of 7.5°, which is still acceptable for a thorough interpretation of potential fault reactivation (Steffen & Steffen 2021b). Table 1 also contains the measured angles. Angles are calculated assuming an average velocity of 2000 ms^{-1}. For some faults we

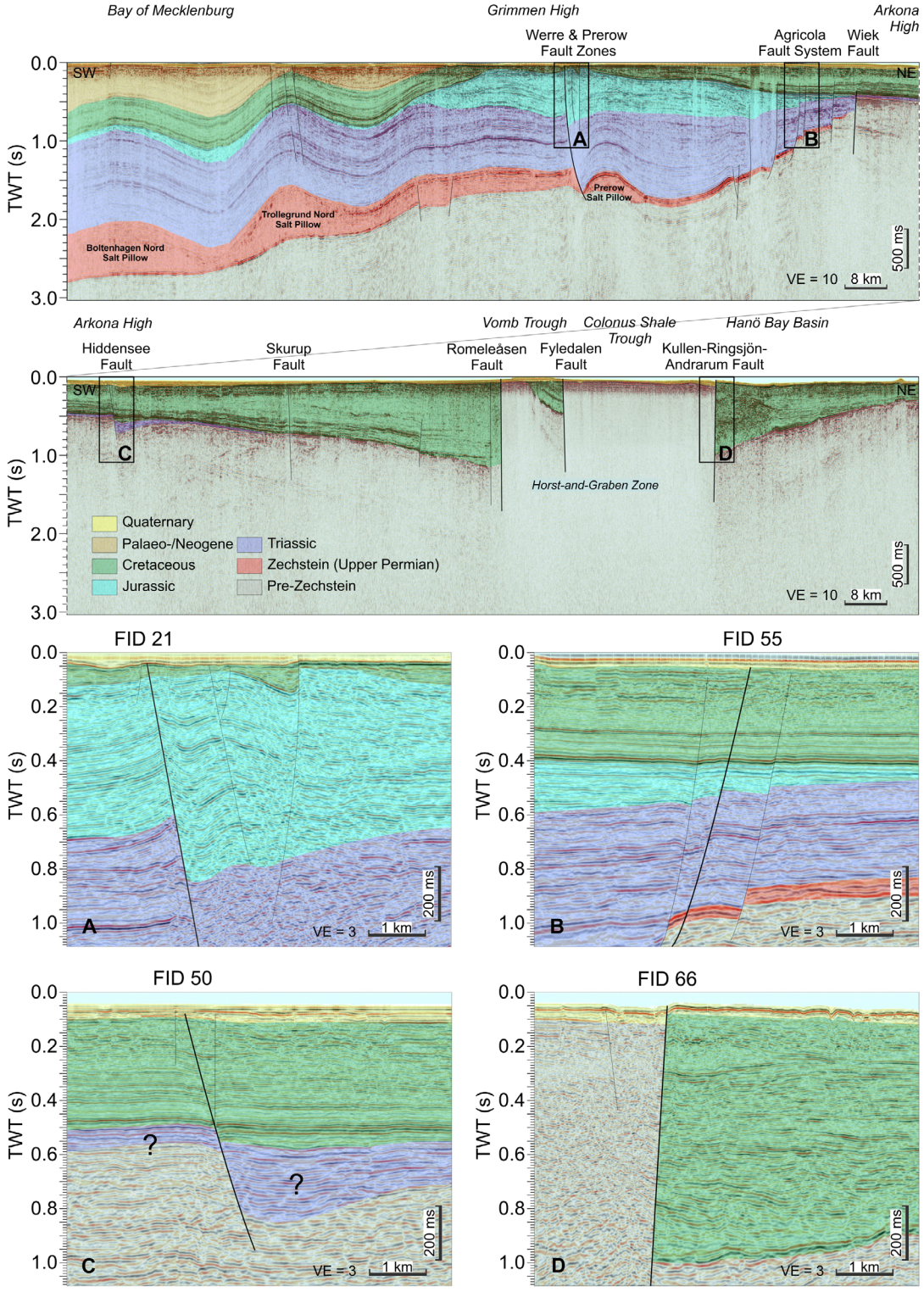

Fig. 4. Seismic section (in two-way travel time), crossing the North German Basin and the horst-and-graben zone (above the STZ) from SW to NE, which shows the prominent displacement of the base of the Quaternary and the sea floor at its northern border. VE = vertical exaggeration assuming an average velocity of 3000 m s^{-1}. For location of the seismic section see Fig. 3.

tested different dip angles either due to a change in the angle with increasing depth, measured in the seismic section, or because the dip angle was not clearly identifiable. If the faults were not crossed perpendicularly by the seismic section, the real dip was calculated using:

Table 1. Measurement points and the estimated properties for identified faults that are discussed in the main text and shown in Fig. 6. For the complete list see Table S1. Each fault has its own number and vertex IDs, for cases in which several measurements with different coordinates were taken along one fault track (EPSG: 25833, ETRS89/UTM zone 33N). Measured strike and dip angles were grouped in 15° multiples (see text). NCFR = number of combinations with potential reactivation for the tested dip angles (values in bold are used for Fig. 6).

FID	Fault ID	Vertex ID	*x* coord.	*y* coord.	Fault name	Strike (°)	Dip angle (°)	App. dip angle range (°)	NCFR per dip angle group						
									0°	15°	30°	45°	60°	75°	90°
2	2	1	190 426	6 104 434		328	53						**24**		
6	6	1	244 905	6 115 235	Langeland F.	120	56	49–67				0	**15**		
13	12	2	197 034	6 066 992	Kieler Bucht-Schönberg VG	14	60						**19**		
35	22	2	325 292	6 047 261	Werre FZ	132	54						**15**		
65	32	9	467 659	5 995 975	Adler Kamień FZ	327	60	34–90			0	0	16		**24**
66	38	1	472 144	6 153 781	Kullen-Ringsjön-Andrarum F.	125	70	60–90					0	21	**24**

$$\gamma = \arctan\left(\frac{\tan \alpha}{\sin \phi}\right) \quad (1)$$

with γ as the actual dip angle, α the apparent dip angle, and φ the crossing direction relative to the fault's strike direction. The number of combinations that point to a potential fault reactivation (NCFR; between 0–34) as obtained by the ΔCFS analysis is shown in Table 1 as well.

Calculation of the change in Coulomb failure stress and the number of parameter combinations that point to a potential fault reactivation

CFS is the distance between the Mohr circle (described by the three principal stress magnitudes) and the failure envelope in a Mohr diagram (Steffen *et al.* 2021b). The change in CFS (ΔCFS) refers to the difference between a CFS at one time point and a CFS at another time point. We estimate ΔCFS by combining glacially induced stresses with lithospheric and tectonic background stresses. The latter are assumed to create a state that is critically stressed at a time point before glaciation started; thus, any additional stress increase would lead to a stabilization or destabilization of the fault. The glacially induced stresses are a combination of three different causes: (i) vertical stresses due to the load itself, (ii) flexural stresses due to the bending of the lithosphere, and (iii) migrating stresses due to the viscoelastic behaviour of the mantle during a glaciation (Steffen *et al.* 2021b). The first stress exists only in regions that are covered by the ice sheet and is zero once the ice is gone. The other two stress components act in the horizontal direction and lead to increased compressional stresses beneath the ice sheet and increased extensional stresses behind the ice margin during the glaciation. Within the bending zone of the crust, in front of the ice margin, the extension is the strongest. Below the neutral line, the character of horizontal stresses is reversed. The third cause of glacially induced stresses arises from the different responses of the lithospheric crust and mantle (upper part of the upper mantle) compared to the viscoelastic upper and lower mantle. The former reacts elastically on GIA time scales (thousands of years), responding instantaneously to ice loading and unloading through the flexing of the lithosphere (Steffen *et al.* 2021b). However, the viscoelastic upper and lower mantle behaves elastically at the beginning of the loading and viscously after the Maxwell time, i.e. the ratio between viscosity and shear modulus, is reached. Stresses that were induced during the early stages of the loading process, when the mantle reacted elastically, migrate to the lithosphere, which reacts elastically during the entire glacial loading process, with continued loading (Steffen *et al.* 2021b). Once the ice sheet is shrinking in size, the horizontal stresses decrease slowly back to zero, which is obtained once the lithosphere has reached isostatic equilibrium. The stress difference (horizontal minus vertical stress) however increases during the melting phase as the vertical stresses have been decreased to zero in regions that were covered by the ice sheet and horizontal stresses still exist. In regions around the ice margin at maximum glaciation, stresses can even change signs several times during the glacial cycle (Steffen & Steffen 2021b). Thus, every potential glacially induced fault must be analysed individually by looking at the change in CFS to study the stress conditions during a glacial cycle.

We estimate the three principal stresses (S1, S2, S3) following Steffen and Steffen (2021b), which requires knowledge about the density of the overlying rocks, gravity, and the stress ratio *R* (Etchecopar *et al.* 1981). The stress ratio *R* varies between 0 and 1 but is unknown in our study area (Heidbach *et al.* 2018). We test three values here (0.05, 0.5, 0.95) to cover a wide range of possibilities. In addition to this, the orientation of $S_{H_{max}}$ is applied to estimate the principal stresses. Based on Ahlers *et al.* (2021, 2022), the stress in the study region is north–south to northwest–southeast directed: thus, we test 60°, 75° and 90° for the orientation of $S_{H_{max}}$ (degree values measured from east in clockwise orientation). Moreover, a strike-slip and a thrust/reverse faulting tectonic background stress regime are considered.

Table 2. Parameter combinations used for the finite element simulations (* = extra dip angles were tested for some faults).

Parameters	Variables	#
Models		
Ice model	ANU-ICE (RSES5, Lambeck *et al.* 2010)	1
Earth model	4× 1D Earth models: (L090_U520_L221, L090_U520_L222, L140_U520_L221, L140_U520_L222) • Lithospheric thickness (LT): 90, 140 km • Upper mantle viscosity (UMV): 5×10^{20} Pa s • Lower mantle viscosity (LMV): 2×10^{21}, 2×10^{22} Pa s 4× 3D Earth models with either 3D lithosphere or 3D mantle (Llat_U520_L221, Llat_U520_L222, L120_SMEAN2, L160_SMEAN2) • 3D lithosphere, UMV 5×10^{20} Pa s and LMV 2×10^{21} Pa s • 3D lithosphere, UMV 5×10^{20} Pa s and LMV 2×10^{22} Pa s • LT 120 km, 3D viscosity based on updated SMEAN2 • LT 160 km, 3D viscosity based on updated SMEAN2	8
Stress and fault parameters in non-optimal cases		
Stress regime	TF/SSF	2
Background stress orientation (S_{Hmax}−angle)	60°/75°/90°	3
Stress ratio R	0.05/0.5/0.95	3
Fault strike	0°/15°/30°/45°/90°/105°/120°/135°/150°/165°	1*
Fault dip	15°/30°/45°/60°/75°/90°	1*
Fault depth	2.5 km	1
Coefficient of friction (μ)	0.6 (standard)	1
Cohesion	0 MPa (not necessary)	1
CFS before glaciation	0 MPa (not necessary)	1
Pore-fluid factor	0 (not tested here)	1

Stresses induced by the last glaciation are calculated with a finite element simulation using the commercial software Abaqus (Dassault Systemes 2021). Here, we follow the method by Wu (2004) for a Cartesian earth model (see Steffen *et al.* 2019, for a detailed explanation of the model setup). We use the ice model by Lambeck *et al.* (2010; ANU-ICE) and eight different earth models (cf. Table 2), all with a horizontal resolution of 50 km. The ANU-ICE model is chosen because it includes the two last glacial cycles. Four of the eight earth models are so-called one-dimensional (1D) earth models where material parameter changes with depth only are considered. In contrast, the other four earth models use a three-dimensional (3D) variation of the lithosphere (based on Wang & Wu 2006) or viscosity variations in the upper and lower mantle based on the 2016 updated version of the seismic tomography model SMEAN2 by Becker and Boschi (2002). The 3D lithosphere model is characterized by a large lithospheric thickness contrast along the Tornquist Zone (see Fig. 8 in Brandes *et al.* 2018). Details about the earth models are listed in Table 2.

Glacially induced stresses are calculated for the eight different GIA models over a time range from 200 ka ago until today (i.e. 1950; following Stuiver & Polach 1977) with timesteps ranging from 3 to 45 000 years. The obtained stresses are combined with 18 background stress states (three $S_{H_{max}}$ orientations times three stress ratios R times two stress regimes). Thus, in total 144 different model–stress combinations (72 for each tested background stress regime) are used to investigate the potential reactivation of the 76 locations distributed across the southern Baltic Sea using the fault parameters listed in Tables 1 and 2. Positive ΔCFS values point to a destabilization of the fault/area (earthquakes are possible), while negative values indicate stable conditions (earthquakes are not likely). We calculate the number of combinations that result in positive ΔCFS values, thus indicating fault reactivation, at some point during the glacial cycles (number of combinations indicating a fault reactivation – NCFR). For each location, the calculation considers the fault strike and dip angles at the location and the 144 model–stress parameter combinations, which represent the uncertainty in our understanding of the subsurface structure and the tectonic background stress situation. The larger the NCFR is, the greater is the potential for fault reactivation at a certain location, because more models and background stress states would result in positive ΔCFS. The NCFR can thus be seen as a measure of how close to optimal orientation a specific fault's strike and dip angle are in relation to the tectonic background stress regime, so that reactivation would be possible when glacially induced stresses are added.

Results

The total NCFR is visualized in Fig. 5. The dominant trend of the faults runs in a northwestern direction, see e.g. the block-terminating faults close to the STZ or the Western Pomeranian Fault System (cf. Fig. 5A,B). Single faults, such as the Gat Fault (western border of the Rønne Graben), the Hiddensee Fault or faults in the northern extension of the Glückstadt Graben trend north-northeast. The dip angle varies (Table 1, Fig. 5A). While faults of the inversion zone in the eastern study area show a very steep dip angle of up to 75°–90°, the Mesozoic, polyphase reactivated structural features in the western working area appear to have flatter dip angles between 45° and 75°.

Two different tectonic background stress regimes were tested: a thrust/reverse-faulting and a strike-slip-faulting one. Assuming a thrust/reverse-faulting background stress field we observed no activation across the working

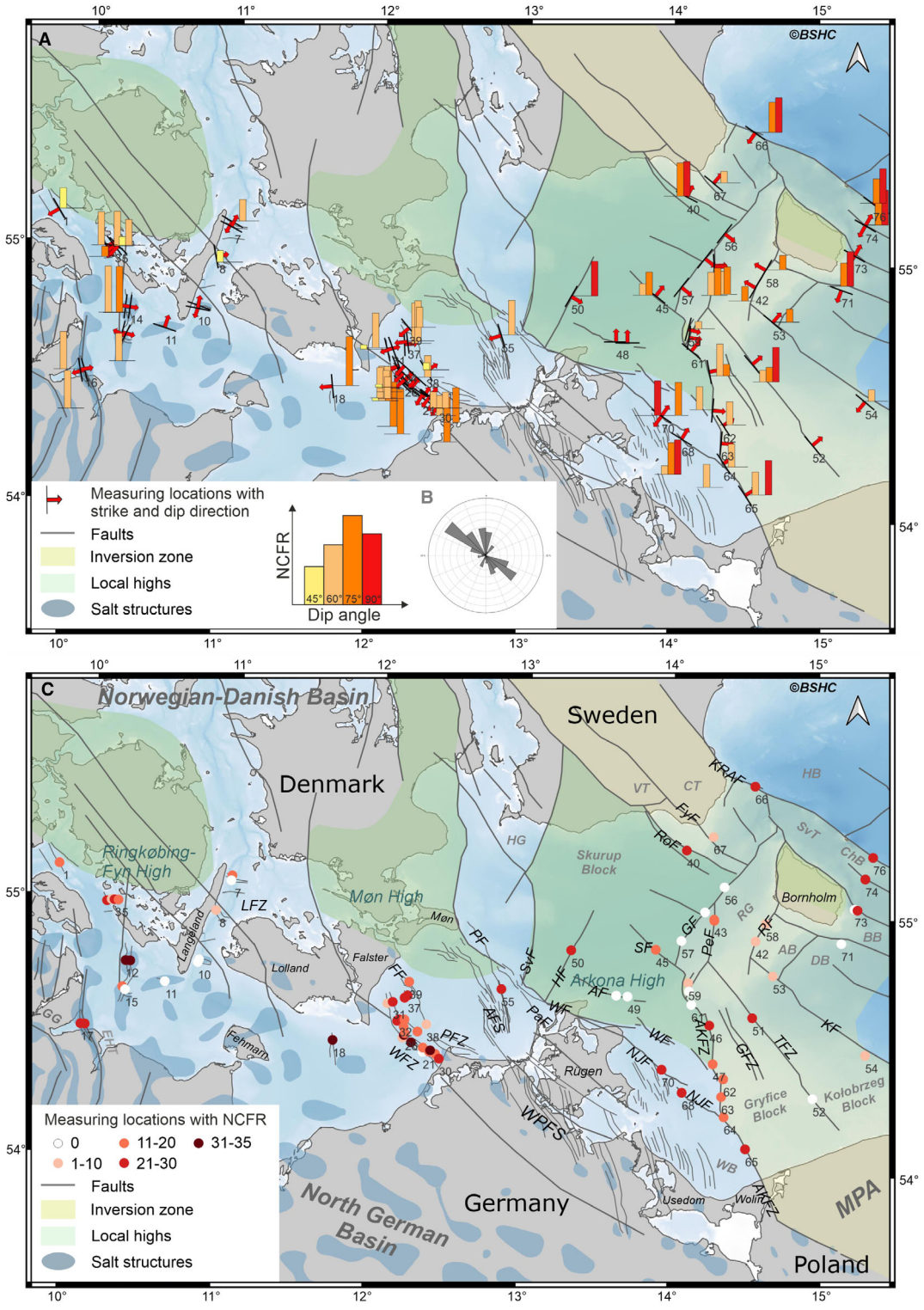

Fig. 5. A. The number of combinations that point to potential fault reactivation (NCFR) in relation to the strike and dip angles at the 76 different measuring sites, assuming a strike-slip background stress. B. The rose diagram represents the dominant northwest–southeast orientated strike direction, the corresponding dip direction trends 90° clockwise (plotted with OpenStereo; Grohmann & Campanha 2010). C. Maximum NCFR at the different measuring sites, assuming a strike-slip background stress (cf. Table S1). For abbreviations and references see Fig. 1. See Figs S3–S5 for close-ups.

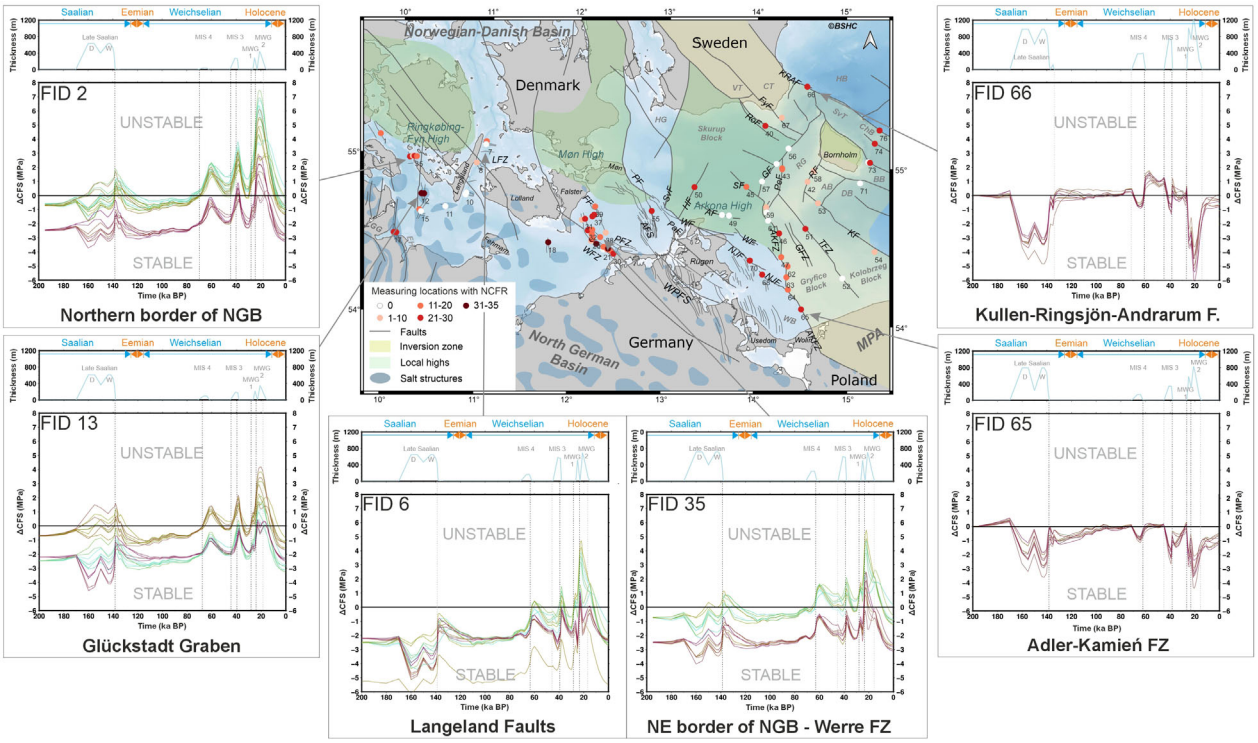

Fig. 6. Comparison of the number of combinations that point to potential fault reactivation (NCFR) across the study area (map in the centre) and over time, starting 200 ka (Late Saalian phase; ΔCFS diagrams). The upper panel in the individual ΔCFS diagrams shows the corresponding ice thickness variation at the location. In the lower panel, the ΔCFS curves are plotted of all combinations that result in an instability or potential reactivation of the fault (ΔCFS > 0 MPa) at some point in time during the last 200 ka. Negative values of ΔCFS point to stable conditions, positive values indicate potential fault instability, especially if a curve rises steeply and reaches values above 2 MPa. Vertical dotted lines are time markers, highlighting the moment of potential reactivation (zero-crossing). Colours of curves are chosen in order of the analysis of the combinations. Any apparent colour groupings are coincidental and should not be further interpreted. For abbreviations within the map and references see Fig. 1.

area, and only at site 73 (FID) ΔCFS values reach between −2 and 0 MPa (cf. Fig. S2). Thus, in the following, we concentrate on the results concerning a strike-slip-faulting background stress regime, which was also preferred for this region by Ahlers *et al.* (2021).

The highest NCFR was determined for FID 18 in the Mecklenburg Bay with 34 of 72 combinations resulting in positive ΔCFS at some point in time (cf. Table S1). Note that ΔCFS for some stress–model combinations is positive several times, which points to several phases of potential fault reactivation (cf. Fig. 6). The NCFR is larger than 0 for most of the FIDs indicating that they were prone to glacially triggered faulting at least once in the last 200 ka (Fig. 5C; Table S1). The northwest to north-northwest trending faults of the Romeleåsen, Fyledalen and Kullen-Ringsjön-Andrarum Faults (FIDs 40, 66, 67), the Adler-Kamień Fault Zone (FIDs 46, 47, 62–65), the Nord Jasmund Fault (FIDs 68, 69, 70), the Werre & Falster Fault Zones (FIDs 19–39), as well as Mesozoic faults in the Bay of Kiel (FIDs 1–5) and also the north-northeast to south-southwest trending Hiddensee Fault (FID 50), and crestal faults in the extension of the Glückstadt Graben (FIDs 16, 17), have NCFRs larger than 10, indicating a moderate to high potential for reactivation (Fig. 5C).

The northwestward-trending segments of the Adler-Kamień Fault Zone (FID 59), the Koszalin Fault (FIDs 53, 54) and the northeast-trending Rønne Fault (FIDs 42, 58) show minor activations. Northwest–southeast trending faults east of Langeland (FIDs 6–8) have no or a low potential for reactivation as indicated by no or only a very few combinations resulting in positive ΔCFS. A few faults, like the east–west trending Arkona Fault (FIDs 48–49), the northern transition from the Adler-Kamień Fault Zone into the Skurup Fault (FID 60, 61), and the northeast–southwest trending Gat Fault (FIDs 41, 56, 57), show no potential for reactivation. In total, 16 sites (FIDs in the table) would have never been reactivated during the glacial cycles.

Figure 6 shows the ΔCFS over the past 200 ka and across the working area. The figure represents exemplary the ΔCFS-time diagrams for six locations (see area map) of different tectonic units, crossing the area from west to northeast. Each ΔCFS diagram shows the individual ice thickness directly above each FID location in the upper panel. The ΔCFS is plotted in the lower panel.

The general ice thicknesses vary at the different FID locations, and we see the highest values in the northeast (e.g. at FID 66 during the MWG 2 with 1200 m). Towards the southwest, or parallel to the ice-flow direction, the ice-sheet thickness is reduced. Thus, the Glückstadt Graben (FID 13) is covered by a thinner ice sheet (400 m during the MWG 2). The differences in ice-sheet thickness and the geographical position also lead to differences during the interstadials. Comparing the plots in Fig. 6 during the LGM and especially between the MWG 1 and MWG 2 advances, it is obvious that a complete ice retreat occurred west of Rügen Island (cf. FIDs 2, 6, 13, 35 in Fig. 6), while at the Adler-Kamień Fault Zone (FID 65) a 300 m, and further north, at the Kullen-Ringsjön-Andrarum Fault (FID 66), even a 650-m-thick ice cap remained. In the following, we present the results for specific regions (according to Fig. 6).

North German Basin (NGB, FID 2)

At the northern border of the NGB, 24 (out of 72 for a strike-slip-faulting background stress regime) different combinations point to a reactivation. The measured strike direction and dip angle are 328°/53°. ΔCFS curves for FID 2 in Fig. 6 that become positive are based on a stress ratio R of 0.05 and cover $S_{H_{max}}$ orientations of 60°, 75° and 90°. ΔCFS is negative before the ice advances as the used fault parameters are not optimal in the assumed stress field (optimal fault parameters would be 0°/90° and 120°/90°, 15°/90° and 135°/90°, and 30°/90° and 150°/90° for $S_{H_{max}}$ of 60°, 75° and 90°, respectively). A ΔCFS of 0 MPa at the onset of glaciation would only be present for optimally orientated faults in a critically stressed crust (see Steffen & Steffen 2021b).

The course of the curves points to at least four phases of fault instability. Some ΔCFS curves cross the zero line at 160 ka for the first time. This concerns mainly curves with 60° and 75° $S_{H_{max}}$. These curves peak, with a maximum value of 2 MPa, at 137 ka ago. At the same time, the ice model shows an ice retreat of the Late Saalian advance between 145 and 137 ka ago. The second phase of potential reactivation starts at 68 ka ago and reaches its peak of slightly more than 2 MPa at 60 ka ago. This concerns the same curves as during the first phase. In comparison with the ice thickness, the moment of zero-crossing correlates with the ice advance of the MIS 4 phase, while the ΔCFS reaches its maximum after the ice retreat. A third phase of fault reactivation is indicated by a very steep increase at around 40 ka ago. Here, more ΔCFS curves cross the zero line, now even containing some combinations with 90° $S_{H_{max}}$. All curves reach their maximum of up to 3.8 MPa at 38 ka ago. The third phase takes place during the ice advance of MIS 3 and again, ΔCFS reaches its maximum at the end of the ice retreat. The fourth phase starts *c*. 30 ka ago and is the most remarkable one as all curves cross the zero line at some point in time. All curves peak at 22 ka ago with ΔCFS values reaching up to 7.5 MPa. After this point, six curves indicate a potential fifth phase of fault instability peaking at 16 ka. These six curves are based on two GIA models with 3D viscosity structure, on a stress ratio R of 0.05 and $S_{H_{max}}$ of 60°, 75° and 90°. In comparison with the ice model, the fourth phase between 30–22 ka ago correlates with the start of the ice advance and the final ice retreat of the MWG 1. Probably, the Norske Is advance also had a far-field effect here. The potential fifth phase is related to the final ice retreat of the MWG 2.

Glückstadt Graben (FID 13)

At the Glückstadt Graben, 19 different combinations point to a reactivation of this fault (orientation of 014°/60°) at least once during the last 200 ka. The general trend of the curves is similar to FID 2 (NGB; Fig. 6). There are four main phases of fault instability, although the first phase can be subdivided into two for some curves. Contemporaneously to the Late Saalian ice advance, some curves indicate a stress built-up, which peaks at about 138 ka ago (moment of final ice regression). A second strong increase of the ΔCFS curves took place at 68 ka ago, at the same time when the MIS 4 ice proceeded. The peak was reached a bit earlier than at FID 2, at 62 ka ago. The third phase at 45 ka ago is contemporaneous with the MIS 3 ice advance. The fourth phase, during the LGM, can be subdivided into up to three peaks. The first one, at 26 ka ago, correlates temporally with the starting MWG 1 ice advance. After a minor decrease, all ΔCFS curves cross the zero line and reach their maximum between 24–20 ka ago with values of up to 4.2 MPa, thus much less than at FID 2. Some ΔCFS curves also indicate a third increase between 20–15 ka ago (end of MWG 2).

Langeland Faults (FID 6)

At the Langeland Faults, 15 different combinations point to a reactivation. We note that we have three locations in the vicinity of Langeland for which we investigated a potential fault reactivation, but only FIDs 6 and 8 indicate a reactivation under a strike-slip background stress regime. FID 6 has an orientation of 120°/56° and shows a potential reactivation for all tested R ratios and $S_{H_{max}}$ of 60°.

The general course of the ΔCFS curves represents again the different glaciation phases but only the last three are accompanied by (some) curves that reach positive values (Fig. 6). The ice advance during the Late Saalian does not initiate fault reactivation. The first crossing of the zero line of four different curves at 63 ka ago is associated with the MIS 4 ice retreat. The second phase peaks *c*. 38 ka ago, which corresponds to the ice retreat of MIS 3. By careful inspection, the third phase during the LGM can be separated into three peaks: the first zero line crossing and minor peak is visible at 28 ka

ago, before the MWG 1 phase. The following maximum at 23 ka ago (between the two last advances) comes with the largest ΔCFS values for most of the curves, reaching values of up to 4.8 MPa and thus comparable in magnitude with those at the Glückstadt Graben (FID 13, Fig. 6). A final peak can be found for five curves, which fits in time to the final MWG 2 ice retreat.

Werre Fault Zone (FID 35)

The Werre Fault Zone consists of several northwest-trending faults dipping towards the northeast or southwest. Seventeen locations on the seismic lines, which we used for strike and dip measurements, indicate fault reactivation during the Quaternary, and only FID 21 has zero NCFR. As an example, we present FID 35 (Fig. 6) with measured strike direction and dip angle of 132°/54°. Here, 15 different combinations point to an activation, restricted to a R ratio of 0.05 and a $S_{H_{max}}$ of 60° or 75°. The course of the curves is similar to FID 6 (Langeland Faults) but the magnitudes are a bit larger. The first phase of potential fault reactivation is indicated during the Late Saalian. After a minor ΔCFS peak that fits with the ice reduction (Drenthe) around 150 ka ago where only two curves reach positive values, the final ice retreat at 138 ka ago caused a strong ΔCFS increase so that around half of the curves exhibit positive ΔCFS values. The second and third phases of potential fault reactivations are related to the MIS 4 ice retreat at 62 ka ago and the MIS 3 termination at 38 ka ago. Similar to the Langeland Faults (FID 6) or the Glückstadt Graben (FID 13), the LGM is accompanied by ΔCFS curves that show up to three distinct peaks (Fig. 6). The ice retreat at 23 ka ago is again accompanied by the largest ΔCFS values of up to 5.5 MPa.

Adler-Kamień Fault Zone (FID 65) and Kullen-Ringsjön-Andrarum Fault Zone (FID 66)

Our selected FID 65 (strike/dip = 327°/90°) represents the Adler-Kamień Fault Zone and lies close to the intersection with the Nord Jasmund Fault. The Δ CFS/time plot of FID 65 (Fig. 6) comprises 24 different combinations (with all three R ratio values and $S_{H_{max}}$ of 90°) that point to potential fault reactivation.

The Kullen-Ringsjön-Andrarum Fault Zone represents the northern border of the Colonus Shale Trough. The selected FID 66 (strike/dip 125°/90°) plot comprises 24 different combinations that point to potential fault reactivation (Fig. 6). Again, all R ratio values are possible but in this case for a $S_{H_{max}}$ of 60°.

Both plots (FIDs 65, 66; Fig. 6) have a similar behaviour of the curves until *c*. 62 ka ago. During that time, there are three phases with positive ΔCFS values. The first phase is represented by some combinations that show positive ΔCFS values (~0.5 MPa) *c*. 200–170 ka ago, thus before the Late Saalian ice advance. After stable conditions during the Late Saalian FID 66 also shows a slight indication of unstable conditions during ice retreat. Until the advancing MIS 4 ice shield, the ΔCFS curves vary between −0.5 and +0.5 MPa. A third phase of distinct potential reactivation corresponds to the time between MIS 4 and MIS 3, starting with the MIS 4 ice retreat at 60 ka ago. Reactivation at FID 66 is also possible for some combinations during the MIS 4 ice advance *c*. 72 ka ago. A fourth phase of reactivation is feasible at the end of MIS 3 at *c*. 38 ka ago. However, only the curves at FID 66 reach positive values of up to 1.2 MPa. After that phase, the curves of FID 65 and FID 66 show a last activation at 28 ka ago, with the beginning of the LGM. After a small peak that correlates with the ones found at the western FIDs, the ice shield grew enormously, reaching a thickness of up to 1000 m (MWG 1) at the northernmost site (FID 66) and of 600 m at FID 65 (Fig. 6). During the MWG 2 an ice thickness of even 850 m (FID 65) to 1200 m (FID 66) was possible. The final MWG 2 retreat was not accompanied by fault reactivation at the Adler-Kamień Fault Zone (FID 65), or in the northern part (FID 66).

Summary of modelling results

The high data coverage across the broad study area and the expanded fault zones allows an investigation of spatio-temporal development of the glacially induced stresses (see Movie S1; based on the ice model by Lambeck *et al*. 2010). During the Late Saalian ice retreat, fault reactivation is possible in the northwest part of the Werre Fault Zone, which then may have affected the locations in the southeast until almost all sites could have been reactivated. Then, stable conditions are first indicated in the north, which eventually spread south until the last few sites in the southeast reached stable conditions *c*. 120 ka ago. During the Eemian and Lower Weichselian, all measuring sites are subject to stable conditions, until the next potential phase of fault reactivation starts in the southeast at *c*. 65 ka ago. Unstable conditions spread towards the northwest until *c*. 55 ka ago. Since then, repeated phases of potential reactivation affect the entire Werre Fault Zone. Similarly, this can be observed across the prominent horst-and-graben zone (east of the study area) governed by the preceding or retreating ice-sheet margin.

Discussion

Why are some faults in the southwestern Baltic Sea prone to potential glacially induced reactivation and some not?

The reactivation potential of a fault is especially influenced by its orientation (strike and dip) within the stress field (here, tectonic, lithostatic, and glacially induced stresses; Steffen & Steffen 2021b). In a strike-slip-faulting stress regime with $S_{H_{max}}$ being between 60°

and 90° as used in here, faults that are critically stressed (optimally orientated faults, ΔCFS = 0 MPa) would have a strike angle between 120° and 210° or 300° and 30°, and a dip angle of 90°. When several angles were tested for one FID location, the number of NCFR increased with the steepness of the dip angle.

A change of the dip direction (75° vs. 90°; tested for the Nord Jasmund Fault – FIDs 69 and 70, or the Christiansö Block – FIDs 74 and 75) has no impact. Only at the northeastern border of the Bornholm Block (FIDs 72 and 73) did we find a different NCFR, but in this case angles below 60° were used in the stress analysis for FID 73 (cf. Table S1). These dip angles are further away from optimal orientation in a strike-slip faulting stress regime and thus glacially induced stresses are not large enough to reactive the low-angle dipping faults (Steffen & Steffen 2021b).

Considering a critically stressed crust where optimally orientated faults have a ΔCFS of 0 MPa (yellow stars in Fig. 7), even other fault orientations can be close to instability (black symbols, Fig. 7) and can thus be reactivated once additional stresses (e.g. glacially induced stresses) are added. Major faults in the southwestern Baltic Sea area are close to the critically stressed state (instability) when a strike-slip-faulting stress regime, a stress ratio R of 0.05 and an orientation for $S_{H_{max}}$ of northwest–southeast are used. Almost all faults have ΔCFS values between −5 and 0 MPa before glaciation (Fig. 7). Only the Arkona Fault (striking 270° and dipping 80°) and the Gat Fault (striking 38° and dipping 75°) are further away from a critically stressed state (CFS < −10 MPa). Glacially induced stresses are not large enough to reactivate these faults, which is also visible in their ΔCFS plots over time (see Fig. S7).

Our analysis favours a strike-slip-faulting tectonic background stress regime, which is in line with the findings of Ahlers *et al.* (2021) and supported by the World Stress Map (Heidbach *et al.* 2018). ΔCFS values in a thrust-faulting stress regime do not cross the zero line, but for some faults, only 1–2 MPa more would be needed to reach this line. We note that such stress differences could be overcome with additional stress changes due to pore-fluid pressure changes, which can reach 7 MPa in a thrust-faulting stress regime (Peikert *et al.* 2022). Hence, future modelling investigations should consider tests with pore-fluid pressure changes to estimate if more faults could have been reactivated due to an interplay of glacially induced stresses and increased pore-fluid pressure, for example, due to meltwater input from the waning ice sheet.

How do the dimension and shape of the ice sheet affect glacially reactivated faulting?

Comparing the results, summarized by Fig. 6, we observed relationships between the NCFR and the location of the fault with respect to the ice-sheet margin. Even in such a small region with an extension of around 300 km, the differences in the ice-sheet model have different effects on the studied faults.

The glacially induced stresses vary depending on the location with respect to the ice-sheet centre. Compressional stresses are induced near the surface beneath the ice sheet, while extensional stresses can be found near the surface between the ice-sheet margin and the peripheral bulge, which develops around an area of subsidence during loading and collapses during unloading. The compressional stresses increase the overall compressional stress setting in the crust, while the extensional stresses decrease the crustal stresses. Thus, depending on which side of the ice margin the fault is located, the effect of the glacially induced stresses can be very different. The southern Baltic Sea was located in the peripheral bulge during ice advances of all glaciation phases, partly at the ice margin during the Weichselian glaciation at glacial maximum (thus with mainly extensional stresses prevailing), and completely covered by several hundred metres of ice during the glacial maximum of the Saalian glaciation (thus with mainly compressional stresses being induced). The response of the faults is different depending on where the fault was located with respect to the ice-sheet margin, which is visualized in Fig. 8 for two locations.

During the ice advance (Fig. 8B), the bending of the lithosphere leads to an internal horizontal extension in front of the ice that decreases the horizontal stresses for the two locations as shown in Fig. 8. However, location 2 (red) lies closer to the advancing ice margin, where the crustal bending and horizontal extension are stronger, compared to location 1 (purple). Thus, the Mohr circle moves towards the line of failure, indicating fault instability. When the area is covered by the ice sheet, glacially induced horizontal stresses become compressional, which increases the total stresses again, resulting in fault stability (both locations in Fig. 8C). As the distance from the fault to the ice-sheet margin increases and the fault is located beneath the ice (e.g. during ice advance), the vertical and horizontal compressional stresses increase, leading to more stable conditions. During ice retreat (Fig. 8D), location 1 (purple) is free of ice earlier than location 2 (red), which leads to a faster decrease of the horizontal stresses. At some point during ice retreat, the minimum horizontal stresses (S3) become extensional again, which results in an increase of the Mohr circle and thus positive ΔCFS values are possible. This change from compressional to extensional stresses happens first for the area that was closer to the ice margin during the glacial maximum, and thus location 1 (purple) is represented by a larger Mohr circle compared to location 2 (red). In addition, the change from compressional to extensional stresses for the minimum principal stress occurs only for regions close to the former ice margin. Nowadays, compressional stresses are prevailing, which leads to stable conditions. Please note that this

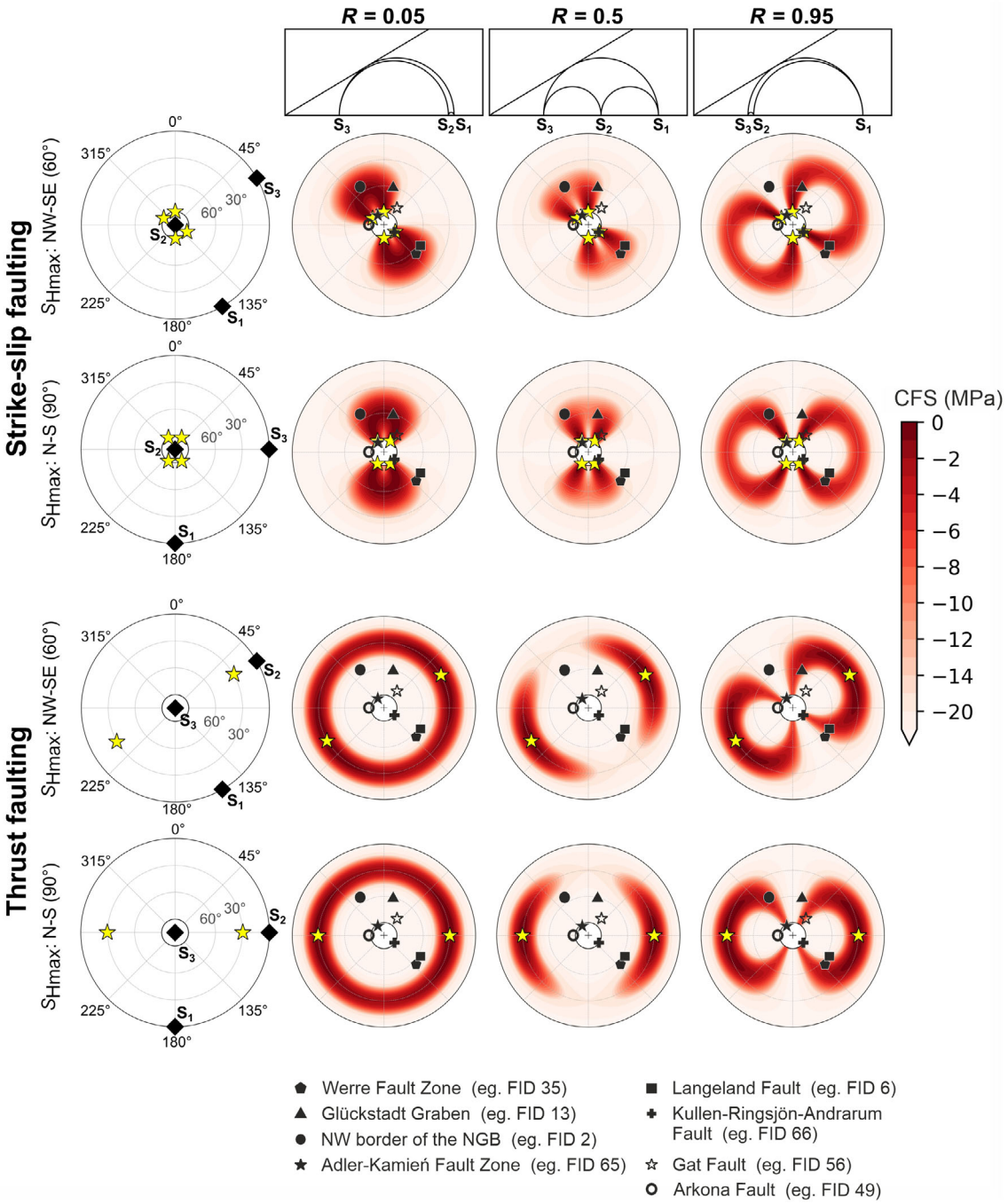

Fig. 7. Polar plots with CFS variations for a critically stressed crust depending on the strike direction and dip angle of optimal (yellow stars) and non-optimal faults. Strike-slip (upper panel) and thrust/reverse (lower panel) faulting background stress regimes are differentiated, as well as three stress ratios (column-wise), illustrated with the corresponding Mohr diagrams (modified after Steffen & Steffen 2021b). The strike direction can be measured at the outer circle with 0° at the top and increasing angle in a clockwise direction. The dip angle increases from the outer part of the circle (0°) towards the centre (90°). Faults are presented in Fig. 6. Symbols with a black fill are potentially reactivated faults, white filled symbols represent faults with no potential for fault reactivation according to our calculations. Faults within the reddish area have a high chance of reactivation due to GIA stress changes.

is only valid for a strike-slip faulting stress regime and other results can be expected for a normal- and thrust/reverse-faulting stress regime.

Relating the above to our study region, we find that the western region of the southern Baltic Sea was covered by a thick ice sheet during the Late Saalian advances, inducing increased compressional stresses, which led to a small increase in ΔCFS when the ice retreated – thus being equivalent to location 2 (red) in Fig. 8. In contrast, the same region was at the edge of the ice sheet during the

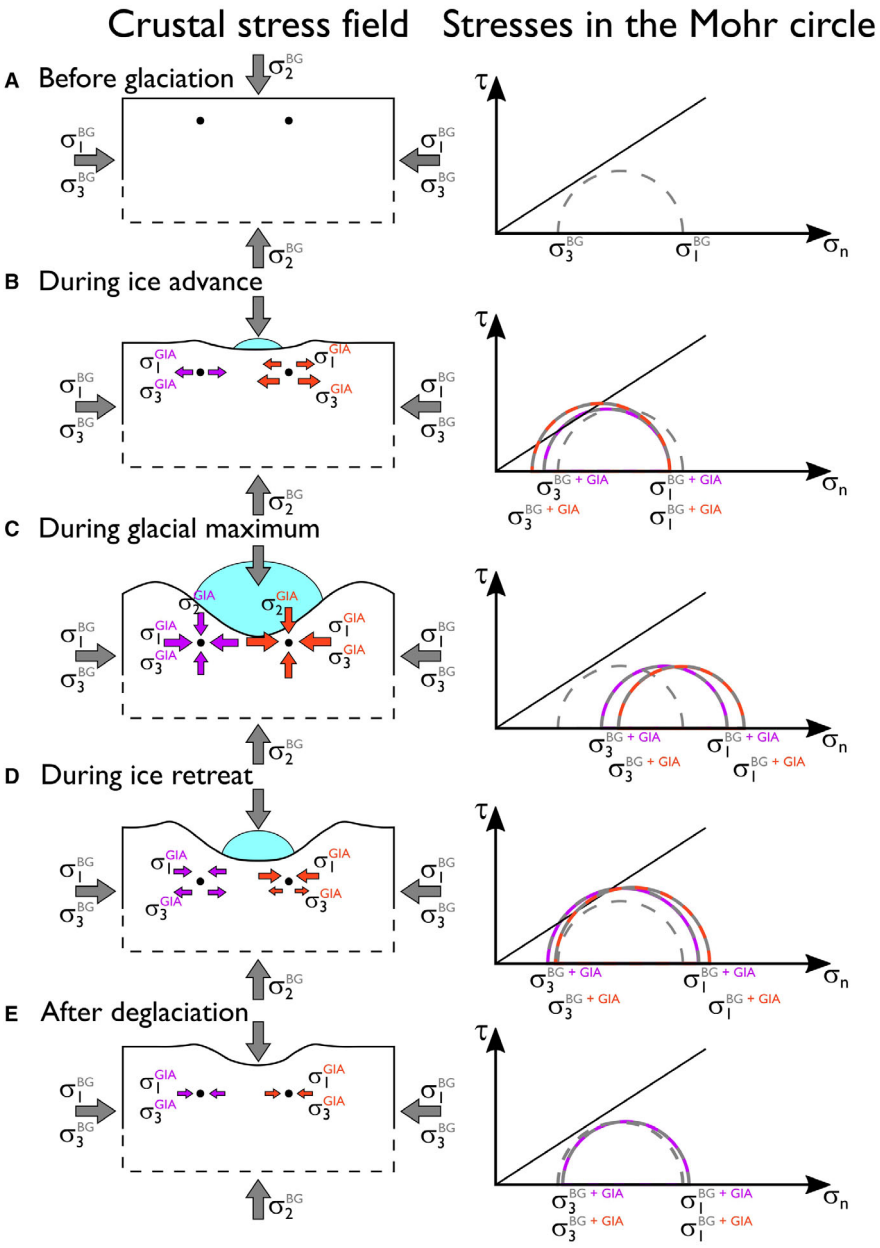

Fig. 8. Conceptual sketch of the relationship of glacially induced stresses in a strike-slip-faulting stress regime at two locations with respect to the ice margin (A–E). We discuss two scenarios in the text. The first scenario mimics stresses in the southwestern (purple) and southeastern (red) Baltic Sea during the Weichselian glaciation. In the second scenario, only stresses in the southwestern Baltic Sea are compared but during the Saalian (red) and Weichselian (purple) glaciations. The Mohr diagram illustrates the induced stresses.

Weichselian glaciation and thus was equivalent to location 1 (purple) in Fig. 8. At this location dominantly extensional stresses were induced, leading to large ΔCFS values during both ice advance and retreat. Similarly, fault locations FID 2 and FID 66 can be correlated with locations 1 (purple) and 2 (red) (Fig. 8), respectively, for all glaciations. The eastern region of the southern Baltic Sea was covered by a thick ice sheet during the Saalian and Weichselian glaciations leading to very low ΔCFS during these glaciations. Only during the MIS 4 and MIS 3 ice advances was the eastern part of the southern Baltic Sea close to the ice margin, leading to more unstable conditions during and after ice retreat. The western region of the southern Baltic Sea had only a very thin ice cover during these advances, which also becomes visible in increased ΔCFS values during ice advance and maximum glaciation as dominantly extensional stresses prevailed at these times.

Differences in the ΔCFS curves for the Late Saalian advances with respect to the more recent ice advances

also stem from the fact that the latter are better known and have a much finer spatial as well as temporal resolution in the ice model ANU-ICE by Lambeck *et al*. (2010) than the former. To summarize, the location of the fault with respect to the ice sheet is very important to consider when analysing glacially induced stresses, and this study shows the importance of detailed ice models to understand their potential to reactivate pre-existing faults. It is expected that ice models of the next generation that are constrained with more and better input data will provide more accurate results.

The earth models considered in this study cover different aspects of horizontal and vertical subsurface variations that are discussed in the GIA-related literature; thus, the resulting curves of temporal stress behaviour can be considered to roughly envelop results from other earth model variations not addressed here. However, the used earth models are still rather coarse and omit interesting details; for example, our models do not include a layer of salt or any other sedimentary and tectonic structures (e.g. layers or graben).

Additional uncertainties for the glacially induced stresses stem from the estimation of the background stresses. The ΔCFS is obtained under the assumption that the crust is critically stressed before glaciation started ($CFS_{\text{before glacation}} = 0$ MPa). While this is observed for various regions in the world (e.g. Oklahoma; Walsh & Zoback 2015), this might have not been the case for the study region prior to the Saalian glaciation. However, stresses must have been close to a critical state in northern Europe before the glaciations as otherwise earthquakes during the Holocene (e.g. Brandes *et al*. 2012, 2015, 2018; Pisarska-Jamroży *et al*. 2019, 2022; Grube 2019a, b; Müller *et al*. 2020) could not be explained. A small deviation from this assumption would lead to a shift of all curves, but reactivations would still be happening due to the high glacially induced stresses modelled here (up to 7.5 MPa in positive ΔCFS). The pore-fluid pressure was also not considered in the stress calculation as it has several uncertainties. The variation in this pressure over time, especially in areas that have undergone ice-sheet growths and shrinking, is unknown to date. Thus, only a constant pore-fluid pressure could be used, which would has, due to its physical definition, no effect on the ΔCFS (Wu 2021).

Is there a certain stress and GIA model combination for which many faults indicate potential glacially induced fault reactivation in the southwestern Baltic Sea?

Various parameters (earth model, stress parameters) were tested here to analyse the stress changes for the southern Baltic Sea. Considering that the studied region is relatively small, measuring 375 km (east–west) by 175 km (north–south), the earth model as well as the stress parameters (*R* ratio and direction of the maximum horizontal stress $S_{H_{max}}$) are not expected to vary significantly within this region. Thus, we can assume that one combination (of all model–stress parameters) gives a positive ΔCFS for all the faults in the study area that show a displacement in the Quaternary. From the 144 different model–stress combinations of all input parameters tested for each measuring point, we identified certain parameter combinations that could have led to many fault reactivations. Figure 9 summarizes exemplarily the NCFR for each model–stress combination at 20 ka ago.

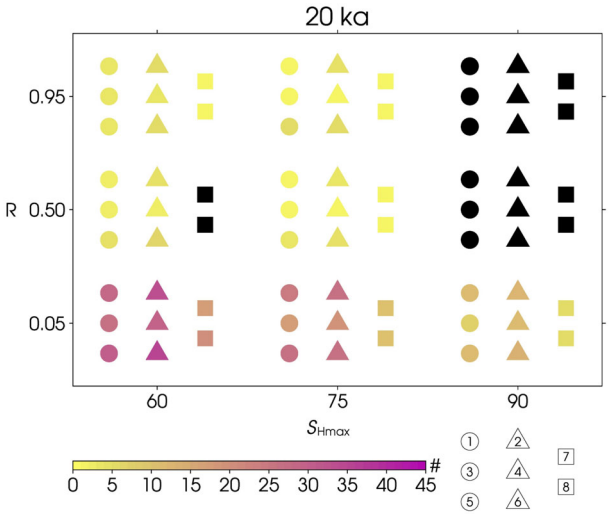

Fig. 9. Number of faults that show positive ΔCFS at 20 ka ago, based on the stress ratio *R*, the orientation of $S_{H_{max}}$ (measured from east in clockwise direction) and the earth model in a strike-slip background stress regime. A black symbol means no fault has been reactivated. Earth model code: 1 = L090_U520_L221; 2 = L090_U520_L222; 3 = 140_U520_L221; 4 = L140_U520_L222; 5 = Llat_U520_L221; 6 = Llat_U520_L222; 7 = L120_SMEAN2; 8 = L160_SMEAN2 (see Table 2 for explanation of the earth model parameters).

The highest number of fault locations that have positive ΔCFS values at 20 ka ago can be found for a strike-slip background stress regime with a $S_{H_{max}}$ orientation of 60° (northwest–southeast, measured from east in a clockwise direction) and a *R* ratio of 0.05. The latter means that the magnitude of the vertical stress is almost the same as the magnitude of the maximum horizontal stress and thus, sufficiently large stress changes (e.g. due to ice advances) could lead to a fault reactivation with normal faulting. A northwest–southeast orientation of $S_{H_{max}}$ in northern Germany was also obtained by Ahlers *et al*. (2021). They found a change in the stress regime from strike-slip-faulting near the surface to normal-faulting for depths below 1500 m. This could be explained by a low *R* ratio where the stress regime can change even with small stress undulations.

Analysing all results over all timesteps, the highest number of potentially reactivated faults is achieved with the earth model Llat_520_L222, a 3D earth model that considers the rheological variability along the suture zone. This suggests that GIA models with a 3D

lithosphere structure should be preferred in glacially induced stress analyses, especially if the potential Quaternary activity of the faults as indicated by this model can be independently confirmed.

Do the results correlate with other glacially induced reactivations discussed in Germany and Denmark?

Most faults in our study area were very likely reactivated at least once during the glaciations of the last 200 ka. However, this requires a strike-slip background stress regime with $S_{H_{max}}$ orientated northwest–southeast ($S_{H_{max}}$ 60°, or to a lesser extent, even 75°) and a *R* ratio of 0.05. Glacially triggered earthquakes were also suggested for the Jasmund Peninsula (Rügen Island, Dwasieden) and the Gnitz Peninsula (Usedom Island), which are located onshore in the southern Baltic Sea area (Pisarska-Jamroży *et al*. 2019, 2022). A reactivation between 24.5 and 23.5 ka for Rügen Island and between 23.6 and 21.5 ka for Usedom Island was obtained with OSL dating of soft-sediment deformation structures and ΔCFS changes from GIA modelling in combination with the same stress field parameters. According to Kenzler *et al*. (2017), the Jasmund Peninsula (Rügen Island) was reached by the first late Weichselian ice advance at 22±2 ka. Hence, the fault reactivation as dated by Pisarska-Jamroży *et al*. (2019, 2022) presumably took place during the ice advance, in front of the ice margin. Also, our results, e.g. for the Nord Jasmund Fault (Fig. S7), the southern part of the Adler-Kamień Fault and west of Rügen Island at the Werre Fault Zone, indicate a reactivation before and after the MWG 1 (Brandenburg advance), and thus support the onshore findings.

Moreover, Pisarska-Jamroży *et al*. (2022) tested further input parameters during their GIA modelling. Similar to our results, the authors inferred a *R* ratio of 0.05 and a north-northwest to south-southeast orientation of $S_{H_{max}}$ with the highest probability for Usedom Island. Furthermore, northwest–southeast trending faults with a dip angle between 60°–75° (cf. polar plots in Fig. 7) showed the most convincing results (Pisarska-Jamroży *et al*. 2022).

Brandes *et al*. (2018, 2022) dated the fault reactivation at the Børglum Fault (Denmark, northern boundary of STZ) pointing to an activity between 14.5–12.0 ka ago (decay of the ice sheet), which agrees with modelling results based on a strike-slip-faulting background stress regime. According to Brandes *et al*. (2022) faults within the STZ show repeated fault activation. Our results support a polyphase glacially induced fault reactivation at the STZ.

Al Hseinat *et al*. (2016) and Huster *et al*. (2020) investigated the 2-km-wide vertex grabens above the Waabs salt wall (Eckernförde Bay). Both studies revealed a Pleistocene fault reactivation due to the advancing and retreating glaciers. Al Hseinat *et al*. (2016) and Huster *et al*. (2020) also suggested that this Pleistocene fault reactivation was accompanied by vertical movements of the salt wall due to ice loading. This idea is supported by other methodological studies, e.g. by Lang and Hampel (2023). Our earth models do not include local crustal differences, for example salt structures. Therefore, we cannot make any statements about glacially induced salt tectonics. However, the crestal graben-terminating faults are represented by our FIDs 16 and 17 (cf. Fig. 5). The ΔCFS/time diagram (Fig. S7) showed clear indicators of an activation, after the Late Saalian advance, in front of the advancing MIS 4 and MIS 3 (both show only a minor ice cover, thus the faults were located within the peripheral bulge), during the advancing MWG 1 and some curves also show a fifth peak during the MWG 2. Thus, our results support a polyphase reactivation of these crestal faults during the Pleistocene and especially during the Late Saalian and Weichselian ice advances as well.

Faults at a greater distance from the former ice margin are in the peripheral bulge and show an activation during the ice retreat and after the deglaciation (Harz Boundary Fault: Müller *et al*. 2020; Osning Thrust: Brandes *et al*. 2012). However, both previously mentioned studies assumed a thrust/reverse faulting background stress regime and optimally orientated faults, which differs from our parameters.

How does a possible reactivation of this multitude of faults fit into the picture of the palaeoseismicity of the area and the present seismicity?

To illuminate this question, we use our best model–stress combination to investigate the ΔCFS development in the next 1000 years (strike-slip background stress regime with $S_{H_{max}}$ orientation of 60°, *R* ratio of 0.05, and the 3D earth model Llat_520_L222). The ice repeatedly advanced and retreated over the area during the last 200 ka. This affected the peripheral bulge, which migrated at some distance from the ice margin. Hence, the individual faults were exposed to all stress scenarios (Fig. 8A–E) at some point in time. During the last glaciation stage, all were situated in the peripheral bulge, which explains their recent potential for fault reactivation (cf. Fig. 2.7 D3 in Steffen *et al*. 2021b). A remaining positive ΔCFS and thus a potential for fault reactivation is indicated for the dominantly northwest–southeast–striking inversion zone (northwest and southeast of Bornholm Island), the Nord Jasmund Fault, some localities of the Werre and Falster Fault Zones, and further measuring points in the northwestern part of the Bay of Kiel (Fig. 10). Interestingly, within the Baltic region this pattern agrees with some recent earthquakes (since AD 800; Deutscher Erdbebenkatalog,©BGR, Hannover 2012, e.g. in the Werre Fault Zone and along the Colonus Shale Trough. The reader should be aware that the plotted earthquake localities in Fig. 10 differ in depth and are of tectonic origin in general. Hence, the present and near future seismicity in the southwestern Baltic Sea might be, to some extent, related to the last glaciation and the ongoing

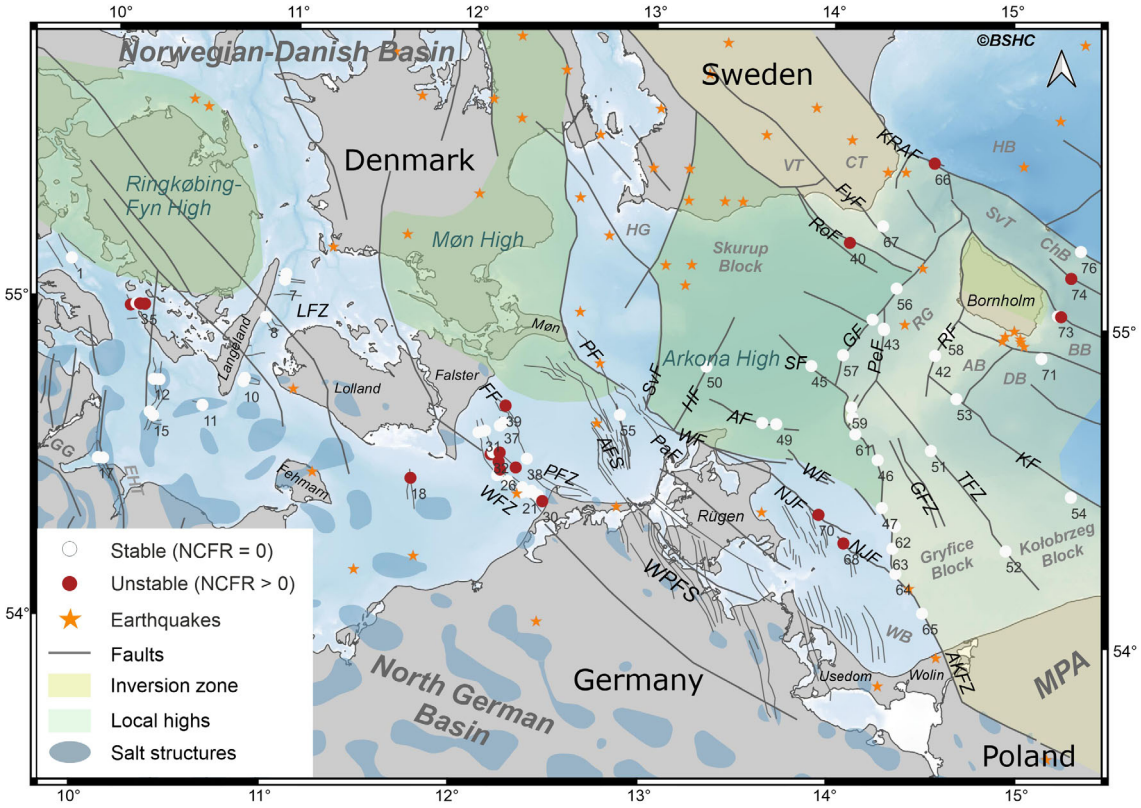

Fig. 10. Locations where fault reactivations are possible within the next 1000 years, calculated with our best model–stress combinations. Dots show the NCFR – red dots represent unstable fault conditions. Only earthquakes of tectonic origin are shown, according to Deutscher Erdbebenkatalog, ©BGR, Hannover (2012). For abbreviations and references see Fig. 1, and Fig. S6 for close-ups.

GIA processes. Of course, there are many other processes that can also affect seismicity, but, at least according to our calculations, GIA cannot be fully excluded as one of the potential trigger mechanisms.

Conclusions

In this study, we determined the strike and dip properties of 44 faults at 76 localities from seismic reflection data collected within the southwestern Baltic Sea and investigated their potential glacially induced reactivation in the last 200 ka. For certain locations, we tested different dip angle values as no precise angle could be determined from the seismic data or the dip angle of a fault changed with increasing depth. The closer the dip angle gets toward the optimum orientation (resulting from the background and glacially induced stresses), the higher the number of combinations that point to potential fault reactivation (NCFR). The maximum NCFR are shown in Fig. 5C. However, the actual angle could deviate from the measured value (within the range shown in Table S1) and thus also the NCFR. This study focusses on comparing and studying the interactions between fault orientation and position, as well as GIA-influenced background stress laterally and temporally.

Using the recommended strike-slip tectonic background stress regime, most of the faults in our study area show a reactivation due to glacial isostatic adjustments (GIA), such as the deep-rooted horst-and-graben structure, close to the Tornquist Zone and the Western Pomeranian Fault System, faults east of Langeland Island, and crestal faults above salt structures, related to the Glückstadt Graben. The strike of these faults differs between northwest and north-northeast, and their dip is steeper than 45°. However, the northeast-trending Gat Fault (west of the Rønne Graben), and the east–west trending Arkona Fault show no activation. As the orientation of $S_{H_{max}}$ of the tectonic stress field varies between 60° and 90°, optimally orientated faults in a strike-slip-faulting stress regime would have a strike angle of 120°–210° or 300°–30°, and a dip angle of 90° (Fig. 7).

Besides the strike and dip parameters, there are other factors to be considered in the calculation of the ΔCFS. The highest potential for fault reactivation occurs when we consider a strike-slip background stress regime with a $S_{H_{max}}$ orientation of 60° (northwest–southeast), a R ratio of 0.05 and a 3D earth model with a varying lithospheric thickness especially over the Tornquist Zone (Fig. 9).

The ΔCFS/time diagrams indicated four to five different reactivation phases in the working area (Fig. 6): Late Saalian phase (170–135 ka), MIS 4 and MIS 3 (70–60 ka, 45–38 ka) and LGM (26–14 ka), all Weichselian advances. However, due to the reduced ice thickness in the southern working area, the LGM is divided into several ice advances (in this study summarized as MWG 1 and 2; with complete ice retreat in between in the south of the study area). Thus, a fifth phase affecting the northern mainland of Germany (south of the working area) is indicated by the diagrams and conceivable. Our results indicate that the activation of faults takes place in front of the ice margin and within the peripheral bulge, primarily during ice retreat, and only secondly during the ice advance.

The highest GIA-induced stress changes occur in the western part of the southern Baltic Sea, during the Weichselian and especially during the MWG 1 glaciation (ΔCFS up to 7.5 MPa). In the northeast, during the Late Saalian advance and the LGM we find a reduced ΔCFS, which is increased in the MIS 4 phase (ΔCFS up to 2 MPa). The number of combinations indicating a fault reactivation varies across the whole area with no clear tendency. However, e.g. the Werre Fault Zone, and the crestal grabens above salt structures show the highest NCFR.

A potential fault reactivation is influenced by an interplay of fault orientation, their location with respect to the ice margin and the type of background stress regime (Fig. 8). The direction of ice advance is also decisive. As the Quaternary ice sheets iteratively advanced from the north and northeast through the Baltic depression, most of the on-average northwest–southeast orientated faults were prone to reactivation.

Furthermore, glacially induced faulting is not (intuitively) predictable (Fig. 10). Detailed earth and ice models, as well as stress parameters, are necessary. We tested several reasonable model–stress combinations, and our results clearly show that a glacially induced influence on the current seismicity pattern in the southwestern Baltic Sea cannot be excluded. A fault reactivation during future glaciations, however, is still only imperfectly predictable due to knowledge gaps in the potential ice distribution and large uncertainties regarding background stress parameters used here (e.g. stress direction and ratio) and beyond (e.g. pore-fluid pressure).

The fault systems studied here could be examined in detail thanks to the high seismic data density that can be achieved at sea. As the fault systems continue into the hinterland of Denmark, Germany, Poland, and Sweden, a reactivation of the faults in the hinterland and during the coming ice ages by GIA can also not be excluded. Moreover, one may even argue that it is highly likely. It will have to be examined whether a potential reactivation of the faults could have an influence on long-term storage facilities for highly radioactive waste if they are planned to be set up at locations that will be covered with several hundred metres of ice again in the future.

Acknowledgements. – The authors declare that they have no conflict of interest. We would like to thank Kurt Lambeck and Anthony Purcell for providing the ANU-ICE history. We are grateful to Volker Klemann for fruitful discussions during the 2023 Glacial Isostatic Adjustment Training School, and to the reviewers Peter Sandersen and Alf Grube for their helpful and constructive comments. We thank IHS Markit for providing KINGDOM seismic interpretation software under the umbrella of the University Grant Program. Moreover, we thank AspenTech for providing Paradigm/EPOS Software Package licences via the Academic Software Program (https://www.aspentech.com/en/academic-program) to support the Federal Institute for Geosciences and Natural Resources (BGR) as a national geological service in non-profit work for the public and education. We used OpenStereo, which is kindly provided as an open source software (https://igc.usp.br/openstereo). This study is part of the StrucFlow Project, which is funded by the Deutsche Forschungsgemeinschaft (DFG, German Research Foundation) grant 96 852 626. This study further contributes to the research topic 'Causes and impacts of climate changes in the Earth system' of the Center for Earth System Research and Sustainability (CEN; University of Hamburg). Open Access funding is enabled and organized by Project DEAL. The authors would like to thank Volkmar Damm and his team from the BGR for providing equipment and expertise for seismic data acquisition during RV 'Maria S. Merian' expedition MSM52. The seismic data set of the MSM 52 survey and the German Earthquake Catalogue (GERSEIS) can be explored and downloaded within the Geoviewer of the Geoportal of the BGR (https://geoportal.bgr.de). The shown seismic section is also available from the BGR (https://www.geo-seas.eu/report/2633203). The bathymetry data, shown in all maps, is based on Baltic Sea Hydrographic Commission (2013). The Danish structural features can be explored within the GEUS' Deep Subsurface Data Portal (https://eng.geus.dk/products-services-facilities/data-and-maps/subsurface-data-denmark).

Author contributions. – ES: Investigation; methodology; visualization; writing – original draft; writing – review and editing. HS: Data curation; investigation; methodology; visualization; writing – original draft; writing – review and editing. RS: Data curation; investigation; methodology; visualization; writing – original draft; writing – review and editing. NA: Investigation; methodology; visualization; writing – original draft; writing – review and editing. CH: Data curation; funding acquisition; project administration; supervision; writing – original draft; writing – review and editing.

Data availability statement. – The seismic data set of the MSM 52 survey and the German Earthquake Catalogue (GERSEIS) can be explored and downloaded within the Geoviewer of the Geoportal of the Federal Institute for Geosciences and Natural Resources (BGR; https://geoportal.bgr.de). The shown seismic section is also available from the BGR (https://www.geo-seas.eu/report/2633203). The bathymetry data, shown in all maps, is based on Baltic Sea Hydrographic Commission (2013). The Danish structural features can be explored within the GEUS' Deep Subsurface Data Portal (https://eng.geus.dk/products-services-facilities/data-and-maps/subsurface-data-denmark) (accessed 30.10.2024).

References

Adams, J. 1989: Postglacial faulting in eastern Canada: nature, origin and seismic hazard implications. *Tectonophysics 163*, 323–331.

Ahlers, S., Henk, A., Hergert, T., Reiter, K., Müller, B., Röckel, L., Heidbach, O., Morawietz, S., Scheck-Wenderoth, M. & Anikiev, D. 2021: 3D crustal stress state of Germany according to a data-calibrated geomechanical model. *Solid Earth 12*, 1777–1799.

Ahlers, S., Röckel, L., Hergert, T., Reiter, K., Heidbach, O., Henk, A., Müller, B., Morawietz, S., Scheck-Wenderoth, M. & Anikiev, D.

2022: The crustal stress field of Germany: a refined prediction. *Geothermal Energy 10*, 10. https://doi.org/10.1186/s40517-022-00222-6.
Ahlrichs, N., Hübscher, C., Andersen, T. R., Preine, J., Bogner, L. & Schäfer, W. 2023a: The Langeland Fault System unravelled: quaternary fault reactivation along an elevated basement block between the North German and Norwegian–Danish basins. *Boreas 52*, 381–401.
Ahlrichs, N., Hübscher, C., Noack, V., Schnabel, M., Damm, V. & Krawczyk, C. M. 2020: Structural evolution at the Northeast North German Basin margin: from initial Triassic salt movement to Late Cretaceous-Cenozoic remobilization. *Tectonics 39*, e2019TC005927. https://doi.org/10.1029/2019TC005927.
Ahlrichs, N., Noack, V., Hübscher, C., Seidel, E., Warwel, A. & Kley, J. 2021: Impact of Late Cretaceous inversion and Cenozoic extension on salt structure growth in the Baltic sector of the North German Basin. *Basin Research 34*, 220–250.
Ahlrichs, N., Noack, V., Seidel, E. & Hübscher, C. 2023b: Salt tectonics in intracontinental sedimentary basins: Triassic–Jurassic salt movement in the Baltic sector of the North German Basin and its relation to post-Permian regional tectonics. *Basin Research 35*, 1433–1459.
Al Hseinat, M. & Hübscher, C. 2014: Ice-load induced tectonics controlled tunnel valley evolution – instances from the southwestern Baltic Sea. *Quaternary Science Reviews 97*, 121–135.
Al Hseinat, M. & Hübscher, C. 2017: Late Cretaceous to recent tectonic evolution of the North German Basin and the transition zone to the Baltic Shield/southwest Baltic Sea. *Tectonophysics 708*, 28–55.
Al Hseinat, M., Hübscher, C., Lang, J., Lüdmann, T., Ott, I. & Polom, U. 2016: Triassic to recent tectonic evolution of a crestal collapse graben above a salt-cored anticline in the Glückstadt Graben/North German Basin. *Tectonophysics 680*, 50–66.
Anjar, J., Adrielsson, L., Larsen, N. K., Möller, P. & Barth, K. 2014: Weichselian history of the Fennoscandian ice sheet in southern Sweden and the southwestern Baltic Basin. *Boreas 43*, 608–626.
Anjar, J., Larsen, N. K., Björck, S., Adrielsson, L. & Filipsson, H. L. 2010: MIS 3 marine and lacustrine sediments at Kriegers Flak, southwestern Baltic Sea. *Boreas 39*, 360–366.
Baltic Sea Hydrographic Commission 2013: *Baltic Sea Bathymetry Database version 0.9.3* Downloaded on 17.06.2019. Available at: https://www.bshc.pro/data/ (accessed 30.10.2024).
Becker, T. W. & Boschi, L. 2002: A comparison of tomographic and geodynamic mantle models. *Geochemistry, Geophysics, Geosystems 3*, 2001GC000168. https://doi.org/10.1029/2001GC000168.
BGE - Federal Company for Radioactive Waste Disposal 2024: Treatment, packaging and storage. Available at: https://www.bge.de/en/radioactive-waste/treatment-packaging-and-storage/ (accessed 30.10.2024).
Börner, A., Gehrmann, A., Hüneke, H., Kenzler, M. & Lorenz, S. 2019: The Quaternary sequence of Mecklenburg-Western Pomerania: areas of specific interest and ongoing investigations. *DEUQUA Special Publications 2*, 1–10.
Böse, M., Lüthgens, C., Lee, J. R. & Rose, J. 2012: Quaternary glaciations of northern Europe. *Quaternary Science Reviews 44*, 1–25.
Brandes, C., Polom, U., Winsemann, J. & Sandersen, P. B. 2022: The near-surface structure in the area of the Børglum fault, Sorgenfrei-Tornquist Zone, northern Denmark: implications for fault kinematics, timing of fault activity and fault control on tunnel valley formation. *Quaternary Science Reviews 289*, 107619. https://doi.org/10.1016/j.quascirev.2022.107619.
Brandes, C., Steffen, H., Sandersen, P. B., Wu, P. & Winsemann, J. 2018: Glacially induced faulting along the NW segment of the Sorgenfrei-Tornquist Zone, northern Denmark: implications for neotectonics and Lateglacial fault-bound basin formation. *Quaternary Science Reviews 189*, 149–168.
Brandes, C., Steffen, H., Steffen, R. & Wu, P. 2015: Intraplate seismicity in northern Central Europe is induced by the last glaciation. *Geology 43*, 611–614.
Brandes, C., Winsemann, J., Roskosch, J., Meinsen, J., Tanner, D. C., Frechen, M., Steffen, H. & Wu, P. 2012: Activity along the Osning Thrust in Central Europe during the Lateglacial: ice-sheet and lithosphere interactions. *Quaternary Science Reviews 38*, 49–62.
Brooks, G. R. & Adams, J. 2020: A review of evidence of glacially-induced faulting and seismic shaking in eastern Canada. *Quaternary Science Reviews 228*, 106070. https://doi.org/10.1016/j.quascirev.2019.106070.
Cohen, K. M. & Gibbard, P. L. 2012: Regional chronostratigraphical correlation table for the last 270,000 years. Available at: https://www.nhm2.uio.no/norges/GTS2012_Quaternary-Poster-reg-GSA2012.pdf (accessed 30.10.2024).
Dassault Systemes 2021: Abaqus Unified FEA. Available at: https://www.3ds.com/products-services/simulia/products/abaqus/ (accessed 30.10.2024).
Deutscher Erdbebenkatalog,©BGR, Hannover 2012: German Earthquake Catalogue, GERSEIS (last update 15.05.2024). Available at: https://geoportal.bgr.de/mapapps/resources/apps/geoportal/index.html?lang=en#/datasets/portal/572FF5BD-EA1A-4BE4-9C7C-9F9CF6EC351B (accessed 10.6.2024).
Erlström, M., Thomas, S. A., Deeks, N. & Sivhed, U. 1997: Structure and tectonic evolution of the Tornquist Zone and adjacent sedimentary basins in Scania and the southern Baltic Sea area. *Tectonophysics 271*, 191–215.
Etchecopar, A., Vasseur, G. & Daignieres, M. 1981: An inverse problem in microtectonics for the determination of stress tensors from fault striation analysis. *Journal of Structural Geology 3*, 51–65.
German Stratigraphic Commission 2016: *Stratigraphic Table of Germany 2016: Table plain 100 × 141 cm, (2) Table folded A4*. German Research Centre for Geosciences, Potsdam.
Graversen, O. 2004: Upper Triassic – Cretaceous stratigraphy and structural inversion off-shore SW Bornholm, Tornquist Zone, Denmark. *Bulletin of the Geological Society of Denmark 51*, 111–136.
Gregersen, S., Lykke Andersen, H., Oncescu, M. C., Mocanu, V., Bankwitz, E., Bankwitz, P. & Grünthal, G. 1995: Recent crustal movements and earthquakes in the area of the Tornquist Zone. *Studia Geophysica et Geodaetica 39*, 257–261.
Grohmann, C. H. & Campanha, G. A. 2010: OpenStereo: open source, cross-platform software for structural geology analysis. *AGU Fall Meeting abstracts 2010, IN31C-06*.
Grube, A. 2019a: Palaeoseismic structures in Quaternary sediments of Hamburg (NW Germany), earthquake evidence during the younger Weichselian and Holocene. *International Journal of Earth Sciences 108*, 845–861.
Grube, A. 2019b: Palaeoseismic structures in Quaternary sediments, related to an assumed fault zone north of the Permian Peissen-Gnutz salt structure (NW Germany) – Neotectonic activity and earthquakes from the Saalian to the Holocene. *Geomorphology 328*, 15–27.
Guterch, A., Wybraniec, S., Grad, M., Chadwick, R. A., Krawczyk, C. M., Ziegler, P. A., Thybo, H. & de Vos, W. 2010: Crustal structure and structural framework. *In* Doornenbal, J. C. & Stevenson, A. G. (eds.): *Petroleum Geological Atlas of the Southern Permian Basin Area*, 11–23. EAGE Publications b.v, Houten.
Hansen, M. B., Lykke-Andersen, H., Dehghani, A., Gajewski, D., Hübscher, C., Olesen, M. & Reicherter, K. 2005: The Mesozoic–Cenozoic structural framework of the Bay of Kiel area, western Baltic Sea. *International Journal of Earth Sciences 94*, 1070–1082.
Hansen, M. B., Scheck-Wenderoth, M., Hübscher, C., Lykke-Andersen, H., Dehghani, A., Hell, B. & Gajewski, D. 2007: Basin evolution of the northern part of the Northeast German Basin — insights from a 3D structural model. *Tectonophysics 437*, 1–16.
Heidbach, O., Rajabi, M., Cui, X., Fuchs, K., Müller, B., Reinecker, J., Reiter, K., Tingay, M., Wenzel, F., Xie, F., Ziegler, M. O., Zoback, M.-L. & Zoback, M. 2018: The World Stress Map database release 2016: crustal stress pattern across scales. *Tectonophysics 744*, 484–498.
Houmark-Nielsen, M. 2004: The Pleistocene of Denmark: a review of stratigraphy and glaciation history. *In* Ehlers, J. & Gibbard, P. L. (eds.): *Developments in Quaternary Sciences: Quaternary Glaciations - Extent and Chronology. Part I: Europe*, Vol. 2, 35–46. Elsevier, Amsterdam.
Houmark-Nielsen, M. 2010: Extent, age and dynamics of Marine Isotope Stage 3 glaciations in the southwestern Baltic Basin. *Boreas 39*, 343–359.
Houmark-Nielsen, M. 2011: Chapter 5 – Pleistocene glaciations in Denmark: a closer look at chronology, ice dynamics and landforms. *In* Ehlers, J., Gibbard, P. L. & Hughes, P. D. (eds.): *Developments in*

Quaternary Science: Quaternary Glaciations – Extent and Chronology. A Closer Look, Vol. 15, 47–58. Elsevier, Amsterdam, Oxford.
Houmark-Nielsen, M., Kjaer, K. & Krüger, J. 2005: De seneste 150.000 år i Danmark. Istidslandskabet og naturens udvikling. *Geoviden 2*, 1–20.
Hübscher, C., Ahlrichs, N., Allum, G., Behrens, T., Bülow, J., Krawczyk, C., Damm, V., Demir, Ü., Engels, M., Frahm, L., Grzyb, J., Hahn, B., Heyde, I., Juhlin, C., Knevels, K., Lange, G., Lydersen, I., Malinowski, M., Noack, V., Preine, J., Rampersad, K., Schnabel, M., Seidel, E., Sopher, D., Stakemann, J. M. & Stakemann, J. 2016: *MSM52 BalTec Cruise Report: March 1 – March 28, 2016 – Rostock (Germany) – Kiel (Germany)*. 46 pp. Hamburg.
Hübscher, C., Al Hseinat, M., Schneider, M. & Betzler, C. 2019: Evolution of contourite systems in the late Cretaceous Chalk Sea along the Tornquist Zone. *Sedimentology 66*, 1341–1360.
Hübscher, C., Hansen, M. B., Triñanes, S. P., Lykke-Andersen, H. & Gajewski, D. 2010: Structure and evolution of the Northeastern German Basin and its transition onto the Baltic Shield. *Marine and Petroleum Geology 27*, 923–938.
Hübscher, C., Lykke-Andersen, H., Hansen, M. B. & Reicherter, K. 2004: Investigating the structural evolution of the western Baltic. *Eos, Transactions American Geophysical Union 85*, 115.
Hughes, A. L. C., Gyllencreutz, R., Lohne, Ä. S., Mangerud, J. & Svendsen, J. I. 2016: The last Eurasian ice sheets – a chronological database and time-slice reconstruction, DATED-1. *Boreas 45*, 1–45.
Huster, H., Hübscher, C. & Seidel, E. 2020: Impact of Late Cretaceous to Neogene plate tectonics and Quaternary ice loads on supra-salt deposits at Eastern Glückstadt Graben, North German Basin. *International Journal of Earth Sciences 109*, 1029–1050.
Kammann, J., Hübscher, C., Boldreel, L. O. & Nielsen, L. 2016: High-resolution shear-wave seismics across the Carlsberg Fault zone south of Copenhagen – implications for linking Mesozoic and late Pleistocene structures. *Tectonophysics 682*, 56–64.
Keilhack, K. 1912: Die Lagerungsverhältnisse des Diluviums in der Steilküste von Jasmund auf Rügen. *Jahrbuch der Preussischen Geologischen Landesanstalt 33*, 114–158.
Kenzler, M., Rother, H., Hüneke, H., Frenzel, P., Strahl, J., Tsukamoto, S., Li, Y., Meng, S., Gallas, J. & Frechen, M. 2018: A multi-proxy palaeoenvironmental and geochronological reconstruction of the Saalian-Eemian-Weichselian succession at Klein Klütz Höved, NE Germany. *Boreas 47*, 114–136.
Kenzler, M., Tsukamoto, S., Meng, S., Frechen, M. & Hüneke, H. 2017: New age constraints from the SW Baltic Sea area – implications for Scandinavian Ice Sheet dynamics and palaeo-environmental conditions during MIS 3 and early MIS 2. *Boreas 46*, 34–52.
King, G. C. P., Stein, R. S. & Lin, J. 1994: Static stress changes and the triggering of earthquakes. *Bulletin of the Seismological Society of America 84*, 935–953.
Kley, J. 2018: Timing and spatial patterns of Cretaceous and Cenozoic inversion in the Southern Permian Basin. *Geological Society, London, Special Publications 469*, 19–31.
Kley, J. & Voigt, T. 2008: Late Cretaceous intraplate thrusting in central Europe: effect of Africa-Iberia-Europe convergence, not Alpine collision. *Geology 36*, 839–842.
Krauss, M. & Mayer, P. 2004: The Vorpommern fault system and its regional structural relationships to the trans-European fault. *Zeitschrift für Geologische Wissenschaften 32*, 227–246.
Krzywiec, P. 2009: Devonian–Cretaceous repeated subsidence and uplift along the Teisseyre–Tornquist zone in SE Poland — insight from seismic data interpretation. *Tectonophysics 475*, 142–159.
Krzywiec, P., Kramarska, R. & Zientara, P. 2003: Strike-slip tectonics within the SW Baltic Sea and its relationship to the inversion of the Mid-Polish Trough—evidence from high-resolution seismic data. *Tectonophysics 373*, 93–105.
Krzywiec, P., Kufrasa, M., Poprawa, P., Mazur, S., Koperska, M. & Ślemp, P. 2022: Together but separate: decoupled Variscan (late Carboniferous) and Alpine (Late Cretaceous–Paleogene) inversion tectonics in NW Poland. *Solid Earth 13*, 639–658.
Lambeck, K., Purcell, A., Zhao, J. & Svensson, N.-O. 2010: The Scandinavian Ice Sheet: from MIS 4 to the end of the Last Glacial Maximum. *Boreas 39*, 410–435.
Lang, J. & Hampel, A. 2023: Deformation of salt structures by ice-sheet loading: insights into the controlling parameters from numerical modelling. *International Journal of Earth Sciences 112*, 1133–1155.
Lang, J., Hampel, A., Brandes, C. & Winsemann, J. 2014: Response of salt structures to ice-sheet loading: implications for ice-marginal and subglacial processes. *Quaternary Science Reviews 101*, 217–233.
Larsen, N. K., Knudsen, K. L., Krohn, C. F., Kronborg, C., Murray, A. S. & Nielsen, O. B. 2009: Late Quaternary ice sheet, lake and sea history of southwest Scandinavia – a synthesis. *Boreas 38*, 732–761.
Litt, T., Behre, K.-E., Meyer, K.-D., Stephan, H.-J. & Wansa, S. 2007: Stratigraphische Begriffe für das Quartär des norddeutschen Vereisungsgebietes. *E&G Quaternary Science Journal 56*, 7–65.
Mazur, S., Krzywiec, P., Malinowski, M., Lewandowski, M., Aleksandrowski, P. & Mikołajczak, M. 2018: On the nature of the Teisseyre-Tornquist Zone. *Geology, Geophysics & Environment 44*, 17. https://doi.org/10.7494/geol.2018.44.1.17.
Mazur, S., Mikolajczak, M., Krzywiec, P., Malinowski, M., Buffenmyer, V. & Lewandowski, M. 2015: Is the Teisseyre-Tornquist Zone an ancient plate boundary of Baltica? *Tectonics 34*, 2465–2477.
Menning, M. 2018: Die Stratigraphische Tabelle von Deutschland 2016 (STD 2016)/ The Stratigraphic Table of Germany 2016 (STG 2016). *Zeitschrift der Deutschen Gesellschaft für Geowissenschaften 169*, 105–128.
Meschede, M. & Warr, L. N. 2019: *The Geology of Germany: A Process-Oriented Approach*. 304 pp. Springer International Publishing, Cham.
Müller, U. 2007: Warnow Formation. *In* LithoLex (Online-Datenbank), Hannover, BGR. Last updated 05.12.2007 (cited 24.01.2023). Record No.1006014. Available at: https://litholex.bgr.de (accessed 30.10.2024)
Müller, K., Polom, U., Winsemann, J., Steffen, H., Tsukamoto, S., Günther, T., Igel, J., Spies, T., Lege, T., Frechen, M., Franzke, H.-J. & Brandes, C. 2020: Structural style and neotectonic activity along the Harz Boundary Fault, northern Germany: a multimethod approach integrating geophysics, outcrop data and numerical simulations. *International Journal of Earth Sciences 109*, 1811–1835.
Müller, K., Winsemann, J., Tanner, D. C., Lege, T., Spies, T. & Brandes, C. 2021: Glacially induced faults in Germany. *In* Steffen, H., Olsen, O., Sutinen, R. & Olesen, O. (eds.): *Glacially-Triggered Faulting*, 283–303. Cambridge University Press, Cambridge.
Narkiewicz, M., Maksym, A., Malinowski, M., Grad, M., Guterch, A., Petecki, Z., Probulski, J., Janik, T., Majdański, M., Środa, P., Czuba, W., Gaczyński, E. & Jankowski, L. 2015: Transcurrent nature of the Teisseyre–Tornquist Zone in Central Europe: results of the POLCRUST-01 deep reflection seismic profile. *International Journal of Earth Sciences 104*, 775–796.
Nielsen, L. H. 2003: Late Triassic – Jurassic development of the Danish Basin and the Fennoscandian Border Zone, southern Scandinavia. *Geological Survey of Denmark and Greenland Bulletin 1*, 459–526.
Olesen, O., Olsen, L., Gibbons, S. J., Ruud, B. O., Høgaas, F., Johansen, T. A. & Kværna, T. 2021: Postglacial faulting in Norway. *In* Steffen, H., Olsen, O., Sutinen, R. & Olesen, O. (eds.): *Glacially-Triggered Faulting*, 198–217. Cambridge University Press, Cambridge.
Overeem, I., Weltje, G. J., Bishop-Kay, C. & Kroonenberg, S. B. 2001: The Late Cenozoic Eridanos delta system in the Southern North Sea Basin: a climate signal in sediment supply? *Basin Research 13*, 293–312.
Pan, Y., Seidel, E., Juhlin, C., Hübscher, C. & Sopher, D. 2022: Inversion tectonics in the Sorgenfrei–Tornquist Zone: insight from new marine seismic data at the Bornholm Gat, SW Baltic Sea. *GFF 144*, 71–88.
Peikert, J., Hampel, A. & Bagge, M. 2022: Relative importance of poroelastic effects and viscoelastic relaxation for postseismic velocity fields after normal and thrust earthquakes: insights from 2D finite-element modelling. *Tectonophysics 838*, 229477. https://doi.org/10.1016/j.tecto.2022.229477.
Pharaoh, T. C., Dusar, M., Geluk, M. C., Kockel, F., Krawczyk, C. M., Krzywiec, P., Scheck-Wenderoth, M., Thybo, H., Vejbæk, O. V. & Van Wees, J. D. 2010: Tectonic evolution. *In* Doornenbal, J. C. & Stevenson, A. G. (eds.): *Petroleum Geological Atlas of the Southern Permian Basin Area*, 25–57. EAGE Publications b.v, Houten.

Philippi, E. 1906: Über die Dislokationen der Kreide und des Diluviums auf Rügen. *Zeitschrift der Deutschen Geologischen Gesellschaft 58*, 119–120.

Pisarska-Jamroży, M., Belzyt, S., Börner, A., Hoffmann, G., Hüneke, H., Kenzler, M., Obst, K., Rother, H., Steffen, H., Steffen, R. & van Loon, T. 2019: The sea cliff at Dwasieden: soft-sediment deformation structures triggered by glacial isostatic adjustment in front of the advancing Scandinavian Ice Sheet. *DEUQUA Special Publications 2*, 61–67.

Pisarska-Jamroży, M., Belzyt, S., Börner, A., Hoffmann, G., Kenzler, M., Rother, H., Steffen, R. & Steffen, H. 2022: Late Pleistocene earthquakes imprinted on glaciolacustrine sediments on Gnitz Peninsula (Usedom Island, NE Germany). *Quaternary Science Reviews 296*, 107807. https://doi.org/10.1016/j.quascirev.2022.107807.

Pisarska-Jamroży, M., Woźniak, P. P. & van Loon, A. J. 2021: Glacially induced faulting in Poland. *In* Steffen, H., Olsen, O., Sutinen, R. & Olesen, O. (eds.): *Glacially-Triggered Faulting*, 304–319. Cambridge University Press, Cambridge.

Ponikowska, M., Stovba, S. M., Mazur, S., Malinowski, M., Krzywiec, P., Nguyen, Q. & Hübscher, C. 2024: Crustal-scale pop-up structure at the junction of two continental-scale deformation zones in the southern Baltic Sea. *Tectonics 43*, e2023TC008066. https://doi.org/10.1029/2023TC008066.

Rempel, H. 1992: Erdölgeologische Bewertung der Arbeiten der Gemeinsamen Organisation 'Petrobaltic' im deutschen Schelfbereich (Evalutaion of the petroleum geological work of the consortium Petrobaltic in the German shelf area). *Geologisches Jahrbuch D99*, 3–32.

Sandersen, P. B. E., Gregersen, S. & Voss, P. H. 2021: Lateglacial and postglacial faulting in Denmark. *In* Steffen, H., Olsen, O., Sutinen, R. & Olesen, O. (eds.): *Glacially-Triggered Faulting*, 263–282. Cambridge University Press, Cambridge.

Sauber, J., Rollins, C., Freymueller, J. T. & Ruppert, N. A. 2021: Glacially induced faulting in Alaska. *In* Steffen, H., Olsen, O., Sutinen, R. & Olesen, O. (eds.): *Glacially-Triggered Faulting*, 353–365. Cambridge University Press, Cambridge.

Scheck-Wenderoth, M., Maystrenko, Y., Hübscher, C., Hansen, M. & Mazur, S. 2008: Dynamic of salt basins. *In* Littke, R. & Gajewski, D. (eds.): *Dynamics of Complex Intracontinental Basins: The Central European Basin System*, 307–322. Springer, Berlin, Heidelberg.

Schlüter, H.-U., Best, G., Jürgens, U. & Binot, F. 1997: Interpretation of reflection profiles situated between the Baltic Continental Plate and the Caledonian Basin in the southern Baltic Sea – first results. *Zeitschrift der Deutschen Geologischen Gesellschaft 148*, 1–32.

Seidel, E., Meschede, M. & Obst, K. 2018: The Wiek Fault System east of Rügen Island: origin, tectonic phases and its relationship to the Trans European Suture Zone. *Geological Society, London, Special Publications 469*, 59–82.

Sirocko, F., Reicherter, K., Lehné, R., Hübscher, C., Winsemann, J. & Stackebrandt, W. 2008: Glaciation, salt and the present landscape. *In* Littke, R. & Gajewski, D. (eds.): *Dynamics of Complex Intracontinental Basins: The Central European Basin System*, 233–245. Springer, Berlin, Heidelberg.

Smith, C. A., Ojala, A. E. K., Grigull, S. & Mikko, H. 2021: Dating of postglacial faults in Fennoscandia. *In* Steffen, H., Olsen, O., Sutinen, R. & Olesen, O. (eds.): *Glacially-Triggered Faulting*, 133–150. Cambridge University Press, Cambridge.

Steffen, H. & Steffen, R. 2021a: Indications on glacially triggered faulting in polar areas. *In* Steffen, H., Olsen, O., Sutinen, R. & Olesen, O. (eds.): *Glacially-Triggered Faulting*, 366–380. Cambridge University Press, Cambridge.

Steffen, R. & Steffen, H. 2021b: Reactivation of non-optimally orientated faults due to glacially induced stresses. *Tectonics 40*, e2021TC006853. https://doi.org/10.1029/2021TC006853.

Steffen, H., Olesen, O. & Sutinen, R. 2021a: Glacially triggered faulting: a historical overview and recent developments. *In* Steffen, H., Olsen, O., Sutinen, R. & Olesen, O. (eds.): *Glacially-Triggered Faulting*, 3–19. Cambridge University Press, Cambridge.

Steffen, H., Steffen, R. & Tarasov, L. 2019: Modelling of glacially-induced stress changes in Latvia, Lithuania and the Kaliningrad District of Russia. *Baltica 32*, 78–90.

Steffen, R., Steffen, H., Weiss, R., Lecavalier, B. S., Milne, G. A., Woodroffe, S. A. & Bennike, O. 2020: Early Holocene Greenland-ice mass loss likely triggered earthquakes and tsunami. *Earth and Planetary Science Letters 546*, 116443. https://doi.org/10.1016/j.epsl.2020.116443.

Steffen, R., Steffen, H., Wu, P. & Eaton, D. W. 2014: Stress and fault parameters affecting fault slip magnitude and activation time during a glacial cycle. *Tectonics 33*, 1461–1476.

Steffen, R., Wu, P. & Lund, B. 2021b: Geomechanics of glacially triggered faulting. *In* Steffen, H., Olsen, O., Sutinen, R. & Olesen, O. (eds.): *Glacially-Triggered Faulting*, 20–40. Cambridge University Press, Cambridge.

Steinich, G. 1972: Endogene Tektonik in den Unter-Maastricht-Vorkommen auf Jasmund (Rügen). *Geologie 20*, 1–207.

Štěpančíková, P., Rockwell, T. K., Stemberk, J., Rhodes, E. J., Hartvich, F., Luttrell, K., Myers, M., Tábořík, P., Rood, D. H., Wechsler, N., Nývlt, D., Ortuño, M. & Hók, J. 2022: Acceleration of Late Pleistocene activity of a Central European fault driven by ice loading. *Earth and Planetary Science Letters 591*, 117596. https://doi.org/10.1016/j.epsl.2022.117596.

Stephan, H.-J. 2014: Climato-stratigraphic subdivision of the Pleistocene in Schleswig-Holstein, Germany and adjoining areas – status and problems. *E&G Quaternary Science Journal 63*, 3–18.

Stuiver, M. & Polach, H. A. 1977: Discussion reporting of ^{14}C data. *Radiocarbon 19*, 355–363.

Sutinen, R., Hyvönen, E., Markovaara-Koivisto, M., Middleton, M., Ojala, A. E. K., Palmu, J.-P., Ruskeeniemi, T. & Mattila, J. 2021: Glacially induced faults in Finland. *In* Steffen, H., Olsen, O., Sutinen, R. & Olesen, O. (eds.): *Glacially-Triggered Faulting*, 231–245. Cambridge University Press, Cambridge.

Thybo, H. 1997: Geophysical characteristics of the Tornquist Fan area, northwest Trans-European Suture Zone: indication of late Carboniferous to early Permian dextral transtension. *Geological Magazine 134*, 597–606.

Thybo, H. 2000: Crustal structure and tectonic evolution of the Tornquist Fan region as revealed by geophysical methods. *Bulletin of the Geological Society of Denmark 46*, 145–160.

Thybo, H. 2001: Crustal structure along the EGT profile across the Tornquist Fan interpreted from seismic, gravity and magnetic data. *Tectonophysics 334*, 155–190.

Vejbæk, O. V. & Britze, P. 1994: *Geologisk kort over Danmark. Geological map of Denmark 1:750 000. Top præ-Zechstein (to vejs løbetid og dybde). Top pre-Zechstein (two-way traveltime and depth)*, vol. *45*. 9. DGU, DGU Kortserie, København, https://doi.org/10.22008/FK2/F9DWMB/IMCMD5.

Vestøl, O., Ågren, J., Steffen, H., Kierulf, H. & Tarasov, L. 2019: NKG2016LU: a new land uplift model for Fennoscandia and the Baltic Region. *Journal of Geodesy 93*, 1759–1779.

Voss, P. H., Gregersen, S., Dahl-Jensen, T. & Larsen, T. B. 2017: Recent earthquakes in Denmark are felt over as large areas as earthquakes of similar magnitudes in the Fennoscandian Shield and East European Platform. *Bulletin of the Geological Society of Denmark 65*, 125–134.

Voss, P. H., Larsen, T. B., Ottemöller, L. & Gregersen, S. 2009: Earthquake in southern Sweden wakes up Denmark on 16 December 2008. *Geological Survey of Denmark and Greenland Bulletin 17*, 9–12.

Walsh, F. R., III & Zoback, M. D. 2015: Oklahoma's recent earthquakes and saltwater disposal. *Science Advances 1*, e1500195. https://doi.org/10.1126/sciadv.1500195.

Wang, H. & Wu, P. 2006: Effects of lateral variations in lithospheric thickness and mantle viscosity on glacially induced relative sea levels and long wavelength gravity field in a spherical, self-gravitating Maxwell Earth. *Earth and Planetary Science Letters 249*, 368–383.

Warsitzka, M., Jähne-Klingberg, F., Kley, J. & Kukowski, N. 2019: The timing of salt structure growth in the Southern Permian Basin (Central Europe) and implications for basin dynamics. *Basin Research 31*, 337–360.

Wu, P. 2004: Using commercial finite element packages for the study of earth deformations, sea levels and the state of stress. *Geophysical Journal International 158*, 401–408.

Wu, P. 2021: State-of-the-science review of the stress field during a glacial cycle and glacially induced faulting. (Technical Report No. NWMO-TR-2021-09). Available at: https://www.nwmo.ca/-/media/Reports-MASTER/Technical-reports/NWMO-TR-2021-09-State-of-the-Science-Review-of-the-Stress-Field-during-a-Glacial-Cycle-and-2021-06.ashx (accessed 30.10.2024).

Znosko, J. 1979: Teisseyre-Tornquist tectonic zone: some interpretative implications of recent geological and geophysical investigations. *Acta Geologica Polonica 29*, 365–382.

Zöllner, H., Reicherter, K. & Schikowsky, P. 2008: High-resolution seismic analysis of the coastal Mecklenburg Bay (North German Basin): the pre-Alpine evolution. *International Journal of Earth Sciences 97*, 1013–1027.

Supporting Information

Additional Supporting Information to this article is available at http://www.boreas.dk.

Fig. S1. A. Glacially induced fault reactivation in the southern Baltic Sea, due to ice advances 140 ka ago (Warthe glaciation). The two scales below represent the ice thickness in metres (based on the ice model by Lambeck *et al*. 2010) and the number of combinations with potential reactivation (NCFR) for the sites. Black dots indicate stable conditions at the fault locations. B. Glacially induced fault reactivation in the southern Baltic Sea, due to ice advances 62 ka ago (MIS 4). The two scales below represent the ice thickness in metres (based on the ice model by Lambeck *et al*. 2010) and the number of combinations with potential reactivation (NCFR) for the sites. Black dots indicate stable conditions at the fault locations. C. Glacially induced fault reactivation in the southern Baltic Sea, due to ice advances 38.5 ka ago (MIS 3). The two scales below represent the ice thickness in metres (based on the ice model by Lambeck *et al*. 2010) and the number of combinations with potential reactivation (NCFR) for the sites. Black dots indicate stable conditions at the fault locations. D. Glacially induced fault reactivation in the southern Baltic Sea, due to ice advances 25 ka ago (Main Weichselian glaciation 1). The two scales below represent the ice thickness in metres (based on the ice model by Lambeck *et al*. 2010) and the number of combinations with potential reactivation (NCFR) for the sites. Black dots indicate stable conditions at the fault locations. E. Glacially induced fault reactivation in the southern Baltic Sea, due to ice advances 20 ka ago (Main Weichselian glaciation 2). The two scales below represent the ice thickness in metres (based on the ice model by Lambeck *et al*. 2010) and the number of combinations with potential reactivation (NCFR) for the sites. Black dots indicate stable conditions at the fault locations. F. Glacially induced fault reactivation in the southern Baltic Sea, due to Main Weichselian glaciation 2 ice retreat (13 ka ago last ice retreat). The two scales below represent the ice thickness in metres (based on the ice model by Lambeck *et al*. 2010) and the number of combinations with potential reactivation (NCFR) for the sites. Black dots indicate stable conditions at the fault locations.

Fig. S2. Comparison between the results for a change in Coulomb failure stress (ΔCFS) during the last 200 ka assuming a strike-slip faulting (left) and thrust/reverse faulting tectonic background stress regime (right) for three different examples of fault locations. The fault number is labelled in the figure, for location see Fig. 3. Strike and dip angles are given as measured value and in parentheses the grouped value for calculation.

Fig. S3. Close-ups of the measurement sites according to Fig. 3. Structural units are redrawn according to Vejbæk & Britze (1994), Schlüter *et al*. (1997), Krzywiec *et al*. (2003), Nielsen (2003), Krauss & Mayer (2004), Seidel *et al*. (2018), Warsitzka *et al*. (2019), Ahlrichs *et al*. (2021, 2023b and citations therein), and Ponikowska *et al*. (2024). AB = Arnager Block; AF = Arkona Fault; AFS = Agricola Fault System; AKFZ = Adler-Kamień Fault Zone; BB = Bornholm Block; ChB = Christiansø Block; CT = Colonus Shale Trough; DB = Darłowo Block; EHMB = Eastholstein–Mecklenburg; EHT = Eastholstein Trough; FF = Falster Fault; FyF = Fyledalen Fault; GF = Gat Fault; GFZ = Gryfice Fault Zone; GG = Glückstadt Graben; HB = Hanö Block; HF = Hiddensee Fault; HG = Höllviken Graben; KF = Koszalin Fault; KRAF = Kullen-Ringsjön-Andrarum Fault; LFZ = Langeland Fault Zone; MPA = Mid-Polish Anticlinorium; NJF = Nord Jasmund Fault; PaF = Parchim Fault; PeF = Pernille Fault; PF = Plantagenet Fault; PFZ = Prerow Fault Zone; RF = Rønne Fault; RG = Rønne Graben; RoF = Romeleåsen Fault; SF = Skurup Fault; SvF = Svedala Fault; STZ = Sorgenfrei–Tornquist Zone; SvT = Svaneke Trough; TFZ = Trzebiatów Fault Zone; TTZ = Teisseyre–Tornquist Zone; WB = Wolin Block; WF = Wiek Fault; WFZ = Werre Fault Zone; WPFS = Western Pomeranian Fault System; VT = Vomb Trough.

Fig. S4. Close-ups of the number of combinations that point to potential fault reactivation (NCFR) in relation to the strike and dip angles assuming a strike-slip background stress (according to Fig. 5A). For abbreviations and references see Fig. S3.

Fig. S5. Close-ups of the maximum number of combinations that point to potential fault reactivation

(NCFR) at the different measuring sites, assuming a strike-slip background stress (according to Fig. 5C). For abbreviations and references see Fig. S3.

Fig. S6. Close-ups of locations where potential fault reactivation could be possible within the next 1000 years, calculated with our best model–stress combinations, according to Fig. 10. Dots show the number of combinations that point to potential fault reactivation (NCFR) – red dots represent unstable fault conditions. Only earthquakes of tectonic origin are shown, according to Deutscher Erdbebenkatalog,©BGR, Hannover 2012. For abbreviations and references see Fig. S3.

Fig. S7. Further examples of fault reactivation (for location see Fig. 5). For explanations on how to interpret these diagrams see Fig. 6 and the according chapter ("Results").

Table S1. Measurement points and the estimated properties for identified faults sorted according to their serial number (FID). Each fault has its own number and vertex IDs, in case there had been several measurements at different locations along one fault track (EPSG: 25833, ETRS89/UTM zone 33 N). Measured strike and dip angles were grouped in 15° multiples (see main text). Blue dip angles have been calculated (cf. Eq. 1). NCFR = number of combinations with potential reactivation for the tested dip angles.

Movie S1. Ice motion vs. fault reactivation during the past 200 ka. Panel A represents the advancing and retreating Scandinavian and British–Irish Ice sheets. Panel B shows the close up of the study area. The ice thickness is given in metres, black dots show stable conditions at the fault locations, red dots indicate a positive Coulomb failure stress change and the potential for fault reactivation. The results are based on a strike-slip background stress regime with $S_{H_{max}}$ orientation of 60°, *R* ratio of 0.05, the 3D earth model Llat_520_L222, and the ice model by Lambeck *et al*. (2010).